FABRICATION AND CHARACTERIZATION OF POROUS ALUMINUM AND ZINC VIA SELECTIVE DISSOLUTION OF Al-Zn ALLOYS

By

Elvin G. Estremera-Pérez

A thesis submitted in partial fulfillment of the requirements for the degree of

MASTER OF SCIENCE

In

MECHANICAL ENGINEERING

UNIVERSITY OF PUERTO RICO
MAYAGÜEZ CAMPUS
2013

Approved by:

_____	_____
O. Marcelo Suárez, PhD President, Graduate Committee	Date
_____	_____
Arturo J. Hernández-Maldonado, PhD Member, Graduate Committee	Date
_____	_____
Pedro Quintero, PhD Member, Graduate Committee	Date
_____	_____
Néstor Pérez, PhD Member, Graduate Committee	Date
_____	_____
Alfredo Morales, PhD Representative of Graduate Studies	Date
_____	_____
Ricky Valentín, PhD Acting Chairperson, Mech. Eng. Department	Date

ABSTRACT

Chemical dealloying can be used to fabricate porous metals by removing one or more of the species out of an alloy. Generally, a corrosive electrolyte is used to selectively dissolve a noble element. Alloy concentration, microstructure, applied electric potentials and corrosive medium are the main aspects affecting the morphology of porosity. By controlling these parameters, scientists have been able to design the size of porosity to the extent of creating nanoporous metals. Pores can be tuned between less than 2 nanometers up to the submicron range. Because of their high surface area, these materials can be used as skeletal catalysts. Some metals, like gold, become chemically active once they become nanoporous, while others can be functionalized with a more noble metal to produce catalysts with low precious metal loading.

Porous zinc and porous aluminum have been successfully fabricated via selective dissolution of various Al-Zn alloys. Different Al-Zn alloys ranging from 15 to 70 at. % zinc were cast with fast cooling rates to promote finer microstructure. The alloy specimens were cut and polished prior to the selective corrosion to favor a uniform dealloying process. Sodium hydroxide (NaOH) and nitric acid (HNO_3) solutions were used to selectively remove the aluminum and zinc atoms respectively. An electrical potential was applied to the samples to increase corrosion energy and help promote porosity formation. Concentration and cooling rate were varied to observe their effect on the attained pore size. The microstructure of the resulting porous sponge was characterized using X-ray diffraction (XRD) and scanning electron microscopy (SEM). The presence and distribution of zinc and aluminum along dendrites were analyzed using energy dispersive X-ray spectroscopy (EDS).

Our results revealed that porosity depends highly on Zn concentration and precursor microstructure resulting from cooling rate upon alloy fabrication. A complete removal of zinc crystals was achieved when Al-Zn alloys were treated with HNO_3. Moreover, a complete removal of aluminum phase was observed when the alloys were corroded in NaOH. EDS results evinced the preferential distribution of zinc around aluminum rich dendrites with some zinc atoms dissolved into the dendrites. This directly affected the morphology of porosity.

RESUMEN

El proceso de des-aleación química puede ser utilizado para crear metales porosos. Esta técnica remueve preferencialmente una especie o un elemento fuera de una aleación. Generalmente se utiliza un medio electrolítico corrosivo para disolver el elemento menos noble. Los aspectos más importantes que afectan la porosidad final son la concentración de la aleación, su microestructura, el potencial eléctrico aplicado y el medio corrosivo. Al controlar estas variables, los científicos han logrado crear metales porosos hasta con porosidad nanométrica. La porosidad puede ser modificada, desde menos de 2nm hasta llegar al rango submicrométrico. El área superficial alta de estos metales les permite ser candidatos ideales para fungir como catalizadores esqueletales. Algunos metales, por ejemplo el oro, se vuelven activos catalíticamente luego de nanoporosos. Otros no activos, luego de ser nanoporosos, se pueden funcionalizar y recubrir con algún material catalítico. Esto crea un material activo con alta área superficial y poca cantidad del mismo.

Aluminio y zinc poroso han sido fabricados exitosamente utilizando el método de disolución selectiva en varias aleaciones de Al-Zn. Aleaciones de Al-Zn con diferentes concentraciones fueron fundidas y enfriadas rápidamente para promover microestructuras pequeñas. Estas concentraciones variaron desde 15 hasta 70 porciento atómico de zinc. Las muestras fueron cortadas y pulidas antes de la corrosión para eliminar efectos superficiales y favorecer una corrosión uniforme. Soluciones de hidróxido de sodio (NaOH) y acido nítrico (HNO_3) fueron utilizadas para remover átomos de aluminio y zinc respectivamente. Un potencial eléctrico fue aplicado para aumentar la energía de corrosión y ayudar a promover la formación de poros. La concentración de las aleaciones y las razones de enfriamiento fueron variadas para observar su efecto en la porosidad obtenida. La microestructura del metal poroso fue

caracterizada utilizando difracción de rayos X (XRD) y microscopio de rastreo electrónico (SEM). La distribución y saturación de zinc y aluminio en las dendritas fueron observadas utilizando espectroscopia de rayos X (EDS).

Nuestros resultados revelan que la morfología de la porosidad depende grandemente de la concentración de zinc en las muestras y de la microestructura obtenida por los métodos de enfriamiento. Une remoción completa de cristales de zinc se logro utilizando HNO_3. Por otro lado, cuando las aleaciones se atacaban con NaOH los cristales de aluminio eran disueltos. Los resultados de EDS evidenciaron la sobresaturación de zinc en las dendritas ricas en aluminio. También permitieron observar la presencia preferencial de átomos de zinc en las fronteras de las mismas. Esta microestructura afecto directamente la morfología final de la porosidad.

DEDICATION

This work is dedicated to my father; Edwin Estremera-Jiménez.

He taught me how to work with my hands and from early age introduced me to materials in his woodworking shop.

Thank you dad.

Este trabajo está dedicado a mi padre; Edwin Estremera-Jimenez

El me ha enseñado a trabajar con mis manos y desde temprana edad aprendí sobre materiales en su taller de ebanistería.

Gracias papá.

ACKNOWLEDGMENTS

This work could have not been possible without the help of God.

"The LORD God is my strength… and he will make me to walk upon mine high places." Habakkuk 3:19

I thank my wife Yeidaliz García for her love, encouragement and patience. She is the best that has happened to me.

I am sincerely thankful to my advisor and friend O. Marcelo Suárez. He not only took the time to guide me through my research and thesis but also gave his wise advice in many personal areas.

I am also thankful to my graduate committee members, Dr. Arturo Hernández-Maldonado, Dr. Pedro Quintero, and Dr. Nestor Pérez for their helpful suggestions and criticism.

I will always be thankful to three great and wonderful students who many times became my hands and eyes in the lab; Amarilis Declet, Rafael Soler and Ronald Valle. We became a team and this work is part theirs.

Thanks to the National Science Foundation for its support under Grant HRD 0833112 (CREST program): *Nanotechnology Center for Biomedical and Energy-Driven Systems and Applications*

TABLE OF CONTENTS

LIST OF FIGURES

LIST OF TABLES

1. INTRODUCTION

In general, nanoporous metals appear to be sponge-like materials with pores sizes ranging from 1nm to 100nm. They are normally composed of two phases: a metallic ligament network and an open cell interconnected structure (pores). *Mesoporous* is the designation given by the IUPAC (International Union of Pure and Applied Chemistry) to those materials bearing pore size between 2 and 50nm while macroporous metals have pores larger than 50nm and microporous ones, smaller than 2nm pores [1]. These materials have special characteristics and properties some being quite unusual. The best known features are their high surface area, the uniform open porosity and their bicontinuous tunable network [1], [2].

Nanoporous metals have been used as catalysts in hydrogenation and in electrocatalytic processes [3]. Some of them offer good biocompatibility while their high surface area and unusual optical properties suggest sensing capabilities. For instance, in the biological field there have been studies trapping laccase inside porous metals to immobilize the enzyme and take advantage of its electrocatalytic activities [4]. More recently nanoporous gold has been found to be a highly active and biocompatible substrate for surface-enhanced Raman scattering [5] whereas nanoporous metal/organic frameworks are being studied to store hydrogen [6].

While there are various ways of manufacturing a nanoporous metal (nanocasting, sacrificial molds, sintering, deposition, etc.) the most studied, easiest to implement and least expensive method is via the selective removal of a species or a specific phase from a metallic solid solution or alloy. This technique, called selective dissolution or dealloying, uses corrosion to dissolve a less noble metallic phase in the alloy.

Historically, aluminum and zinc have been dealloyed from a system after been alloyed to nobler elements. Their low potential (anodic in the galvanic table) made them the best choice to be chemically removed. Since dealloying requires a noble specie and an active one, many of the systems used are based on expensive metals such as gold, platinum and silver. The main challenge of the present work the fabrication of a relatively inexpensive macroporous metal based on aluminum and zinc using chemical dealloying.

Al-Zn alloys were used as precursor materials while casting parameters were analyzed to observe their effect on the final porosity. Two corrosive medium were used, alkali and acid, to observe the corresponding effect on the dissolution process. Additionally, an electric potential was applied to the corrosion process to promote the dealloying and the results were compared to free corrosion.

1.1 LITERATURE REVIEW

Binary alloys can serve as parent materials to fabricate a nanoporous metal when one of the elements in the system is significantly nobler than the other. This creates the possibility of removing the less noble metal chemically while leaving the nobler one “unaltered”. As mentioned before, the selective removal of a single metallic species is called selective dissolution. Recently, the expression *chemical dealloying* has been used as a special type of selective dissolution. Since only one of the metallic elements is dissolved from the binary alloy, the concentration and microstructure of the precursor metal directly affects the final porous structure.

Selective dissolution has been historically studied from the standpoint of corrosion. The undesired presence of porosity in metals leading to failure was the original center of study. Dezincification of brass is the perfect example of how this phenomenon can negatively affect the mechanical properties of a specific alloy. Nowadays, such materials are being studied for a different reason: The characteristic high surface area of nanoporous metals has made them excellent candidates for catalytic applications.

During the 1920s, Murray Raney discovered that “finely divided” Ni specimens could be used as catalysts in hydrogenation of vegetable oil. Raney treated a Ni-Si alloy with sodium hydroxide and the material became more active than the best Ni-based catalysts used at the time [6]. He then added aluminum to the alloy fabricating an even more catalytic material [7]. Raney observed that the solvent was only attacking the other metal in the alloy but not nickel. Finally he noticed how the catalytic activity was intensified by the treatment and studied the resulting porous structure.

For decades, these catalysts were fabricated and used by the industry and the chemical process of ionic dissolution was more or less understood. Yet, the mechanism by which the noble metal makes way for the less noble to ionize and continuously dissolve was not fully understood.

Three mechanisms were originally thought to operate when selectively dissolving a single metal: (I) Ionization-redeposition, (II) volume diffusion, and (III) surface diffusion. In the first mechanism both metals dissolve and then the nobler one gets redeposited. This chemical process was studied by Pickering and Wagner in a Cu-Zn system [8]. Today, the idea of ionization-redeposition has been discarded as the main dealloying mechanism because the nobler element needs a high electrode potential to oxidize while the dissolution can occur at very low potentials.

The second mechanism involves only the ionization of the less noble element while both metals move at the atomic scale. The proposed process was that of vacancy formation in partial steps on the alloy surface and diffusion from the bulk alloy of the less noble metal to the surface meanwhile the nobler would diffuse backwards. This mechanism has also been discarded; as explained by Weissmüller [9], it is not consistent with the rapid kinetics of dealloying. Today, the third mechanism, i.e. surface diffusion, is widely accepted as a suitable way to explain the growth of the bicontinuous porous network. More details about the underpinnings of this third mechanism are presented next.

During the late 1970's, Forty made a series of experiments to observe the micromorphology of gold-silver alloys during selective dissolution [10]. He used transmission electron microscopy (TEM) to witness the live corrosion process and discovered that surface diffusion of gold played a very important role. He observed how gold adatoms would move to agglomerate into gold-rich clusters while freshly exposed silver atoms dissolved. Forty also

developed a model for the parting limit (defined as the minimum amount of the less noble element necessary for dealloying to occur) based on surface diffusion.

More recently, Erlebacher et al. developed a kinetic Monte Carlo model that reproduced all relevant trends of dealloying [11]. The hypothesis was that the phenomenon governing the nanoporous metals characteristic morphology after dealloying was confined to the interface between alloy and electrolyte. The model included diffusion of silver and gold atoms and dissolution of silver. This fundamental work confirmed that surface diffusion was the transport mechanism. Erlebacher also stated the four most important physical characteristics of alloys that may be dealloyed [2]. He did not discover them but rather retrieved them from all the work done throughout the years. These potential systems should comply with four requisites:

1) The species must have a sufficiently large difference in dissolution potentials.
2) The amount of the noble metal in the alloy cannot be too high or too low.
3) The more noble metal must surface-diffuse fast enough in the electrolyte.
4) The parent alloy should be homogenous and stress free.

The requisites listed above allow selecting a proper system to be dealloyed. In effect, since 2001 and following these requisites, many scientific works have been done using dealloying to fabricate nanoporous metals. A large amount of these works use gold alloys [12–18] to fabricate nanoporous gold (NPG). NPG remains one of the most studied nanoporous metals, especially for catalysis applications. In the bulk state, gold has good chemical stability, but once nanoporous it becomes catalytically active. This phenomenon opened the possibilities for many metals, which are known not to be active (in the bulk), to be considered as possible catalysts. Since dealloying works on a system where one of the species is noble and the other is less noble, other systems with similar characteristics have also been studied [19–27].

Aluminum is usually chosen as the material to be removed and remains the most popular choice for most applications [3]. The main reason for its selection is its high activity, gets easily to be alloyed with many desired metals, abundance, and low cost. But the high activity does not necessarily close the possibility for aluminum to become the more noble metal. Because of Erlebacher's requirements a system can be chosen so that with a proper electrolyte aluminum would not ionize.

At the moment of writing this thesis, there were no accounts available in the literature about using aluminum as the noble specie for a dealloying process and no published reports about nanoporous aluminum (NPAl). The present contribution demonstrates that there exists a system where aluminum is the noble metal once, the necessary requirements are met. It also demonstrates that nanoporous aluminum can be fabricated, which creates the possibility of using NPAl as a catalyst.

1.2 OBJECTIVES

The present work focuses on the use of selective dissolution or dealloying for the fabrication of porous zinc and porous aluminum using Al-Zn binary alloys as parent material. It also studies the influence of Al-Zn alloy concentration and microstructure on the final porosity. Finally, the study includes the effect on porosity of different corrosion parameters such as corrosive media and applied voltage upon dissolution.

1.2.1 SPECIFIC OBJECTIVES

- To fabricate porous aluminum and zinc using chemical dealloying from Al-Zn alloy as precursor material
    - To study sodium hydroxide (NaOH) and nitric acid (HNO_3) as corrosive media and observe their effect on porosity morphology.
- To study the effect of solidification cooling rate of the parent alloys on the final porosity after dealloying.
    - To analyze three different cooling media: Water at room temperature (slow cooling rate), iced water (medium cooling rate) and liquid nitrogen (severe cooling rate).
- To dealloy various Al-Zn alloys to analyze the effect of Zn concentration in the final porosity.
    - To identify the concentration that would yield the smallest pore diameter.
- To analyze the effect of applied electrical potential in the corrosion process on the final porosity.

1.2.2 STRUCTURE OF THESIS

In Chapter 2 the theoretical background and state of the art of concerning porous and nanoporous materials and metals is presented. Chapter 3 describes in detail the experimental procedure followed in the fabrication and preparation of samples. It also describes the methods used in the characterization of the samples. Chapter 4 deals with the fabrication of porous aluminum and porous zinc via selective dissolution. It covers two different methods of corrosion and two different electrolytes. It also presents the resulting morphology of porosity. Chapter 4 includes a complete description of findings while the author includes not only the results but also discusses and comments on the findings. In Chapter 5 the characterization of the samples before and after selective dissolution is considered. It includes three general parts: X-ray diffraction, energy dispersive spectroscopy and X-ray mapping results. Chapter 6 enumerates conclusions and gives suggestions for future work.

2 THEORETICAL BACKBROUND

2.1 POROUS MATERIALS

Porous materials are composed of a skeletal solid structure with hollow spaces or pores filled with either gas or liquid. The solid structure can consist of a continuous ligament network or of compacted solid particles. Depending on the type of porosity, they can be classified as either open or closed cell porous materials. Open cell means that the solid skeletal structure forms a frame in which the pores are interconnected, while closed cells refer to isolated closed gas filled pores [28].

The skeletal structure forming the network can be metallic, ceramic, polymeric, or made of any other material or combination of materials. They can be found in nature or can be artificially manufactured and for centuries men have take advantage of their special physical, optical and mechanical properties.

2.2 NANOPOROUS MATERIALS

In recent decades, emerging technologies in the aerospace, chemical and electronic sectors have created the need for advanced porous materials with ever increasingly smaller pores. This miniaturization has reached and even surpassed the nanoscaled boundaries. Novel manufacturing methods such as nanocasting [29], electro and vapor deposition [28], lithography [30] and dealloying are used to manufacture what are called nanoporous materials. These materials may possess completely new properties when compared to their bulk counterpart. Catalysis, filters, sensors and adsorption are some of the many areas where nanoporous materials are being applied. The main feature of these materials is their high surface area. The term *nanoporous* is restrained to materials with pore size between 1 to 100nm. While there are naturally occurring nanoporous materials such as zeolites and clay, scientists have made great efforts to succeed with artificial fabrication. The fabrication of nanoporous materials can result in the complete control of the desire properties. Even though the process of manufacturing a nanoporous material can be very expensive, the manufacturer can control almost every aspect of the final material. The ligament width, pore shape and diameter, geometry of porous structure and chemical properties are some of the characteristics that can nowadays be controlled.

2.3 NANOPORUS METALS

As in other porous materials, nanoporous ones can consist of different materials. Most are oxides or polymers although there is an increasing amount of metallic nanoporous materials. Nanoporous metals can assure better mechanical properties while continuing to serve the described purposes. They can be used as filters or as metallic membranes and some are used as electrodes in electrochemical cells. Interest in nanoporous metals increased when scientists discovered significant changes in the chemical properties of metals once converted to nanoporous ones. For instance, it was observed that the catalytic activity increased in nickel in nanoporous state [7]. Another material that behaves similarly is gold. In the bulk state gold is very chemically stable, but once nanoporous, gold becomes catalytically active and it can be used in various chemical reactions [31] [15].

2.3.1 METHODS OF FABRICATION

There are various methods to manufacture a nanoporous metal. The following section summarizes two of the most common methods.

- Use of sacrificial molds: Polymeric or inorganic porous molds can be used to create a nanoporous metal via replication. The pore morphology is determined by the selected mold. These molds can be easily synthesized and generally have a well-defined geometry. The main advantage of this technique is the precise control on final porosity while the main disadvantage is the high implementation costs.

- Selective dissolution or dealloying: Corrosion can be used to remove a metal form a homogeneous solid solution or an alloy to create porosity. The method consists of selective attacking only one of the species while promoting the evolution of a bicontinuous network. Pore morphology cannot be controlled but concentration and microstructure of precursor alloy can define size of final pores. The main advantages of this technique are the ease of implementation and its relatively low cost.

2.3.2 SELECTIVE DISSOLUTION

As explained above, selective dissolution consists in the selective removal of a metal out of an alloy via electrolytic dissolution. This technique follows the traditional rules of corrosion. One of the metals in the alloy must resist the chemical attack while the other reacts. The specie left to become the nanoporous metal is called the noble specie while the one to be dissolved is called the less noble specie. Nobility depends on the respective electropotentials. Chemists use a list called Galvanic series to classify the nobility of metals. The series or potentials change depending on electrolyte but relative nobility remains approximately the same. Table 2.1 shows a typical galvanic series for seawater. The noble, less active metals are on top (near graphite) while the less noble, more active on the bottom. When selecting a system to be selectively dissolved, care must be taken combining metals. The difference in potentials must be sufficiently high such that the less noble metal reacts galvanically.

Table 2.1 Galvanic series for sea water

Graphite
Palladium
Platinum
Gold
Silver
Titanium
Stainless steel 316 (passive)
Silicon bronze
Stainless Steel 316 (active)
Monel 400
Phosphor bronze
Admiralty brass
Cupronickel
Molybdenum
Red brass
Brass plating
Yellow brass
Naval brass 464
Uranium 8% Mo

Niobium 1% Zr
Tungsten
Stainless Steel 304 (active)
Tantalum
Chromium plating
Nickel (passive)
Copper
Nickel (active)
Cast iron
Steel
Lead
Tin
Indium
Aluminum
Uranium (pure)
Cadmium
Beryllium
Zinc plating (see galvanization)
Magnesium

2.3.3 CHEMICAL DEALLOYING

The process upon nanoporosity evolution (ligament growth by noble metal diffusion) is possible is called dealloying. Both dealloying and selective dissolution involve the selective removal of one of the components from the alloy, but only in dealloying the more noble, non-oxidized specie, is free to diffused along the alloy/electrolyte interface. The following section is a short description of nanoporosity evolution in dealloying as described by Erlebacher et al. [11] [2].

Consider the pit evolution, schematically presented in Figure 2.1. This pit represents a local interface between the evolving nanoporous material and the un-etched alloy. As corrosion progresses, the etching front starts to draw out less noble atoms while leaving behind vacancies coordinated with less noble atoms. The etching front spreads laterally, drawing out all the less

noble atoms in the adjacent monolayer. The remaining untouched noble atoms (now adatoms) start moving along the surface of the alloy agglomerating and coarsening in noble element rich walls of the pit. As they diffuse, fresh less noble atoms begin to ionize enlarging the pit. New noble element rich areas start to grow as the distance to be traveled by diffusing adatoms becomes much longer. This process continues until there are no more less noble atoms available to be ionized. The resulting structure consists of a sponge-like skeleton with interconnected pores.

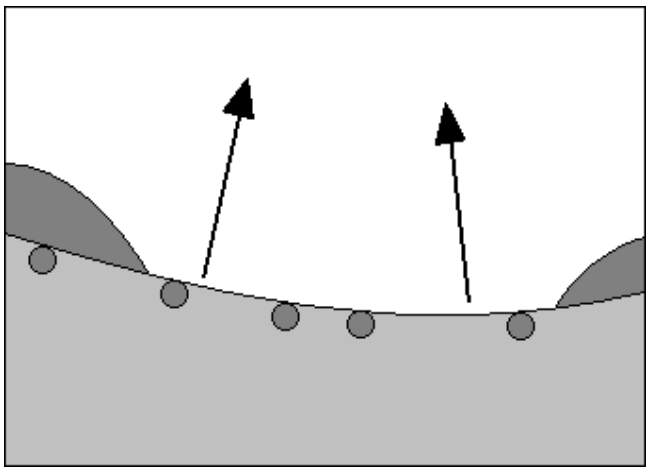

a) Local agglomeration of noble atoms surrounds an interface valley. Less noble atoms dissolve into the electrolyte leaving behind vacancies coordinated with less noble atoms.

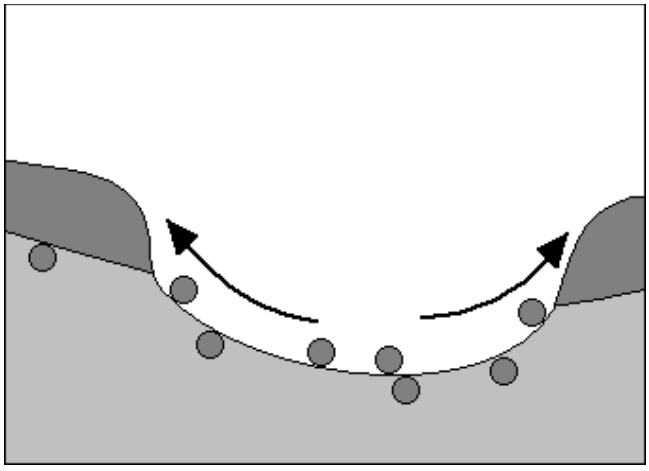

b) Adatoms diffuse along the surface of the alloy agglomerating in noble element rich walls. The once flat valley enlarges as new less noble atoms begin to ionize.

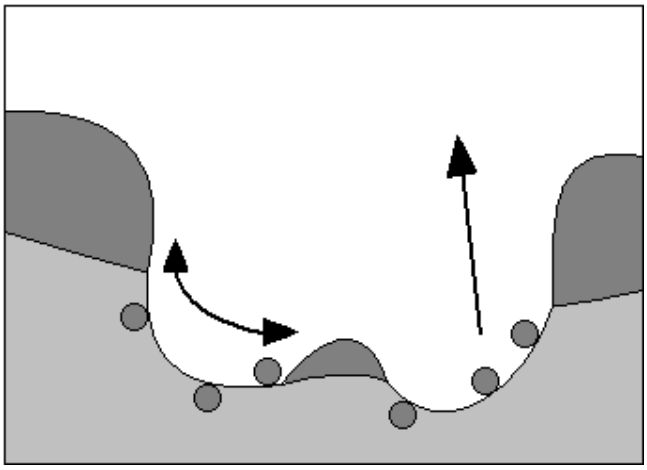

c) New agglomeration areas emerge as the distance to be traveled by adatoms becomes too long. The process continues until there are no more less noble atoms available to be ionized. The surrounding walls become the ligaments of the nanoporous structure.

Figure 2.1 Nanoporous evolution process as described by Erlebacher [2].

3 EXPERIMENTAL PROCEDURE

Since the microstructure of the precursor Al-Zn alloy affects the final morphology of the dealloyed metal, various chemical compositions were investigated in this study. Figure 3.1 shows the corresponding Al-Zn binary phase diagram. Alloy chemical compositions ranging from 15 at. % to 70 at. % Zn in Al (namely 15, 25, 35, 40, and 70 at.%) were fabricated as precursor alloys. 99.5% pure aluminum metal shots from Fisher Scientific™ and 99.9% pure zinc pieces with 2-14 mesh (1.5-7mm in diameter) from Sigma Aldrich™ were weighted to the desired proportions and melted in a graphite crucible at 750ºC. After melting, the liquid was kept at this temperature for 10 minutes, stirring continuously to homogenize the melt. Different cooling techniques followed the melting process.

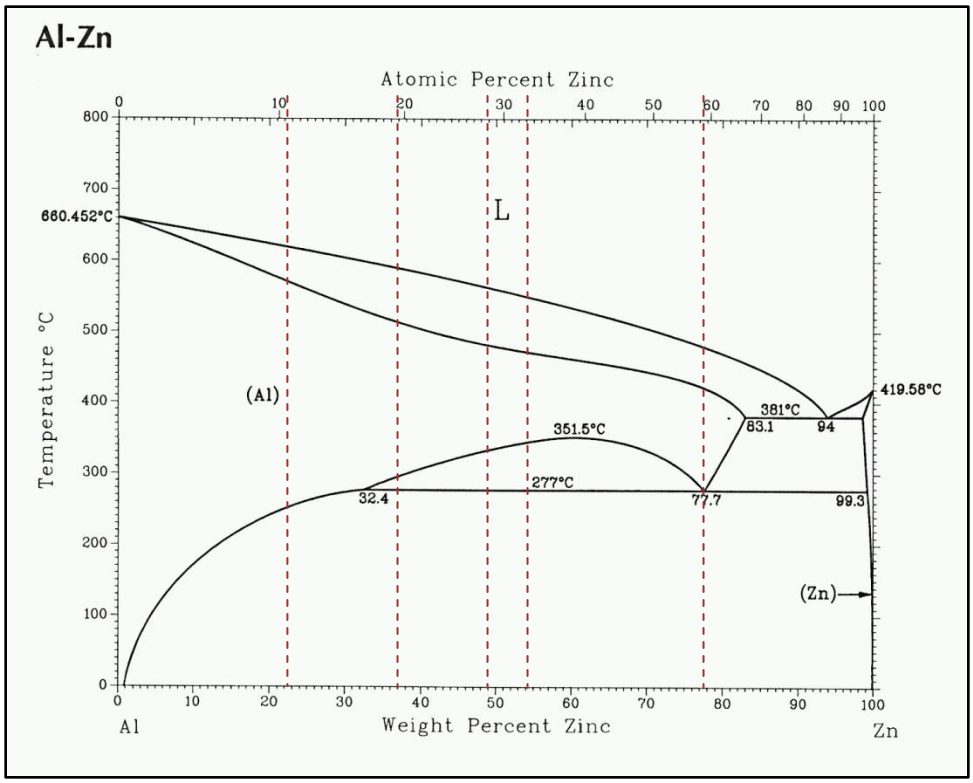

Figure 3.1. Aluminum zinc phase diagram [32].

3.1 SAMPLE QUENCHING

The melt was directly transferred from the crucible to the bath containing the quenching media. Three different cooling rates were selected to study the effect of the precursor microstructure on the porosity. Each alloy composition was quenched individually with the cooling rates resulting in three samples for each chemical composition, i.e. producing three different microstructures. Table 3.1 summarizes the cooling media, their temperatures and the corresponding code name.

Table 3.1 Temperatures and code names for cooling media.

Cooling technique	Temperature [ºC]	Code
Pre-heated mold (control)	300	SC
Water at room temperature quench	27	WQ
Ice water quench	0	IWQ
Liquid nitrogen quench	-200	LNQ

After quenching, a flat surface was machined on the bulk-quenched alloy to facilitate the sample cutting (see figure 3.2). This surface was polished, prior to sample cutting, to promote evenness of the samples. A sample 0.5mm thick was cut using a precision cutting saw. Cutting was the last step before corrosion.

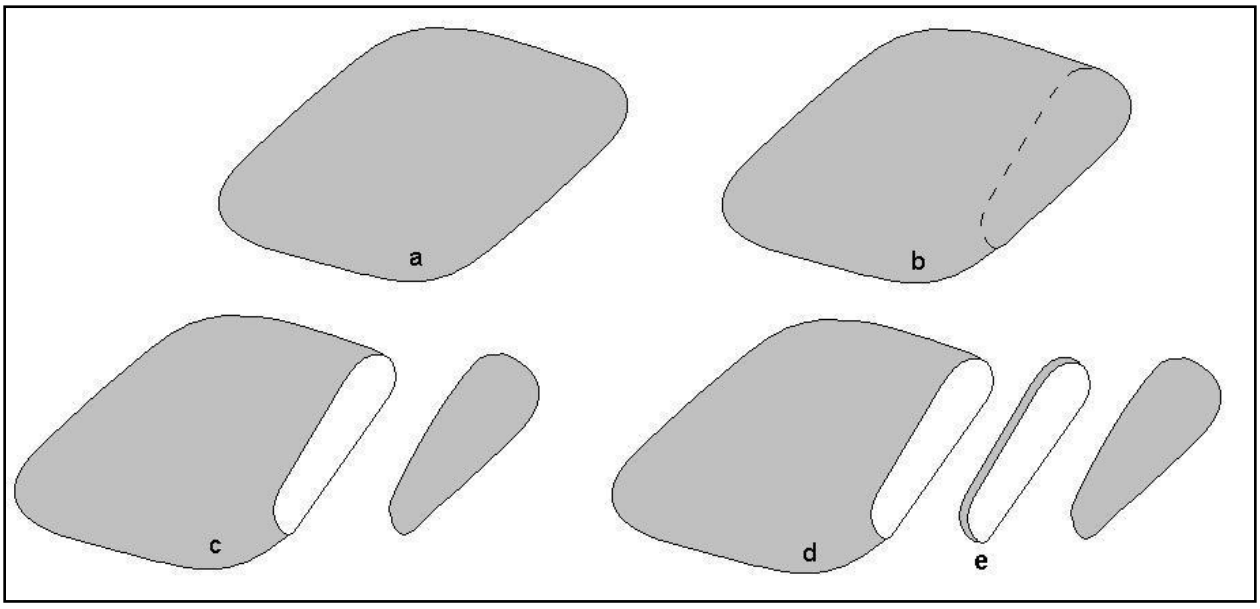

Figure 3.2 Schematic of sample cutting process.
a) Bulk quenched alloy, b) selection of section to be cut, c) flat surface cutting and polishing, d) sample cutting, e) sample.

3.2 CORROSION

For the selective dissolution of aluminum or zinc, two corrosive media were used: alkali and acid. The alkali was a 25 wt. % solution of sodium hydroxide (NaOH) in water while the acid was a 1 wt. % water solution of nitric acid (HNO_3). Two methods of corrosion were used for each electrolyte. The first one, hereon called *free corrosion*, involved only the submersion of the sample into the electrolyte. The second one, hereon noted as *electrochemical corrosion*, involved the application of an electrical potential on the system. For electrochemical corrosion, the sample remained in the electrolyte until no bubbles evolved; an indication that most of the reaction was completed. A graphite rod was used as the positive electrode while the sample was the negative one for electrochemical corrosion (figure 3.3). One DC volt was applied to the system using a power supply. After dealloying, the samples were stored in ethyl alcohol to minimize further oxidation.

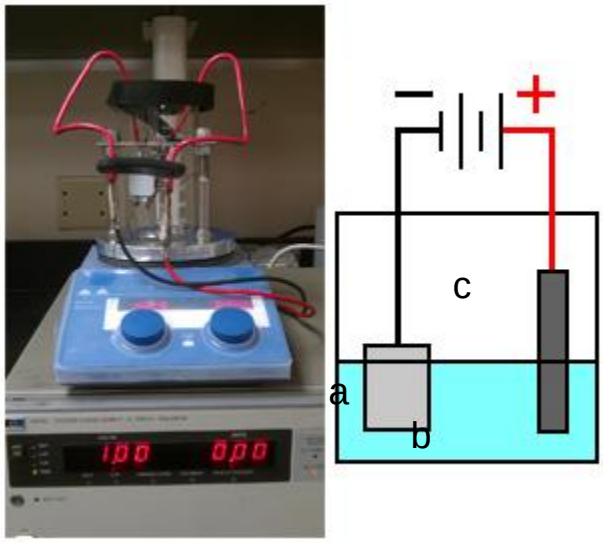

Figure 3.3 Picture and schematic of corrosion cell. a) sample, b) electrolyte, c) graphite electrode.

Figure 3.4 summarizes the process of sample fabrication, preparation and corrosion. Six alloys were cooled with three different quenching methods. Both free and assisted corrosion were used with the two electrolytes described above. This resulted in a total of sixty samples.

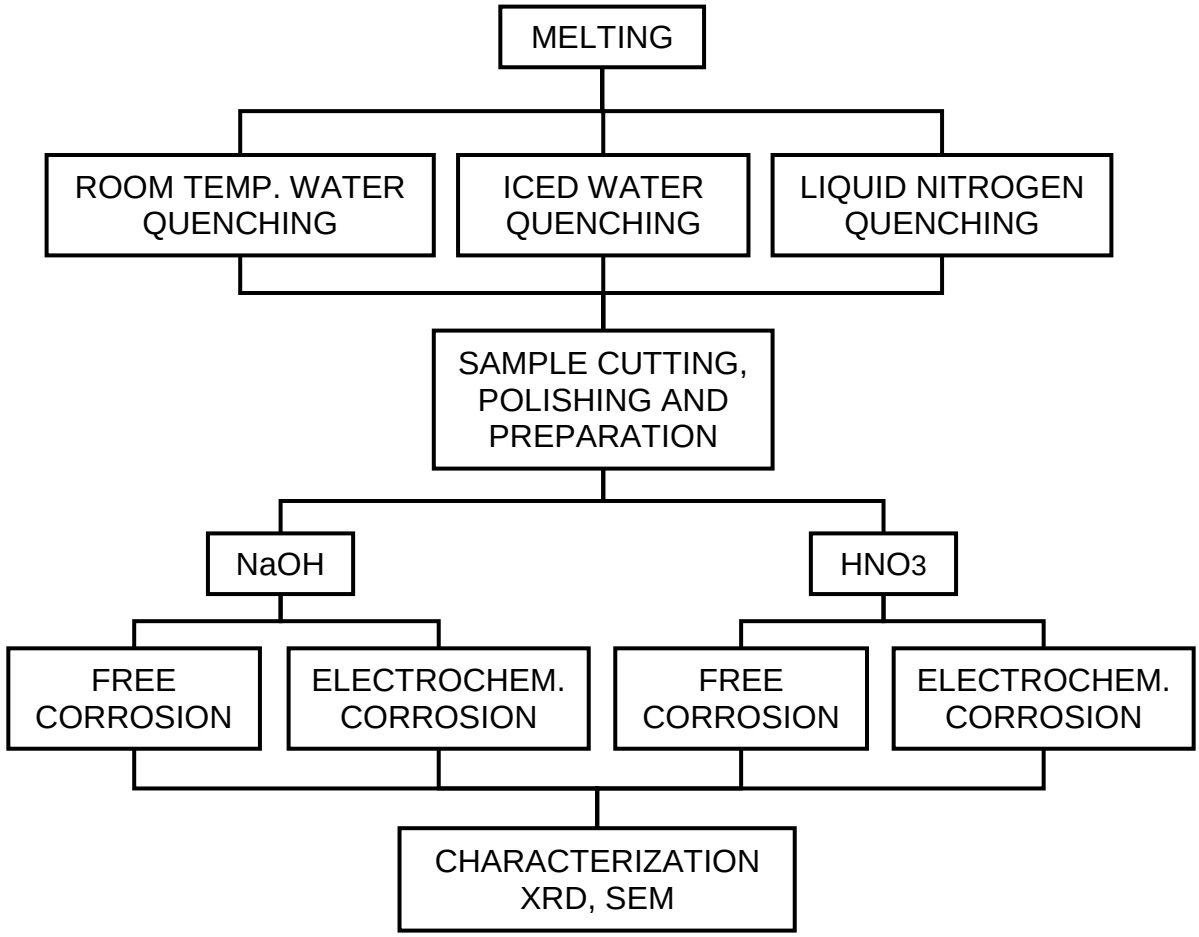

Figure 3.4 Schematic diagram of the experimental procedure.

3.3 CHARACTERIZATION

After corrosion, two main characterization methods were used to study the resulting porous materials: X-ray diffraction (XRD) and scanning electron microscopy (SEM). XRD was used to detect the presence or absence of phases in the treated alloy. It also served as an indirect method to measure the amount of zinc dissolved in solid aluminum prior to the dissolution process. The samples were removed from the storing alcohol and placed with the polished face down onto the XRD sample holder. The resulting diffraction peaks were compared to those of pure aluminum and zinc. Further diffraction analysis helped study zinc solubility in aluminum.

SEM allowed studying the samples microstructure, porous morphology and ligament sizes after corrosion. A thin coating of gold on the surface of the sample helped increase the electrical conductivity of the specimen upon SEM observation. A SEM equipped with an Energy dispersive X-ray spectroscopy (EDX) module permitted further characterization. EDX helped understanding the distribution of zinc along the alloy.

4 FABRICATION OF POROUS Al AND POROUS Zn

4.1 ALLOY PREPARATION

This chapter deals with the aspects concerning Al-Zn alloy selection, preparation and processing. It also gives an explanation on how cooling rates can affect the final porous morphology while describing the different quenching media used in this work.

4.1.1 SELECTION OF REPRESENTATIVE CHEMICAL COMPOSITIONS

The ratio of components in an alloy affects the porosity formation during dealloying [2]. If there is an excessive amount of the less noble metal, most of the alloy would dissolve and no porous structure would evolve. If there is too few of the less noble metal, porosity would be created but in minimal amount. The term “parting limit” defines the minimum amount of the less noble element necessary for dealloying to occur. Even though specific parting limits for most systems remain unknown, it is expected to be within 20 at. % and 60 at. % [2]. In the particular case of Al-Zn system, parting limit has never been studied before.

In order to examine the effect of Zn concentration, five different binary alloys were fabricated as precursor alloys, with the compositions shown in the Al-Zn phase diagram in Figure 4.1. This range of Zn concentration allowed observing the effect of the parent

microstructure on the final porosity. It also provided a hint of where the parting limit can be located, although this was not the purpose of the present thesis.

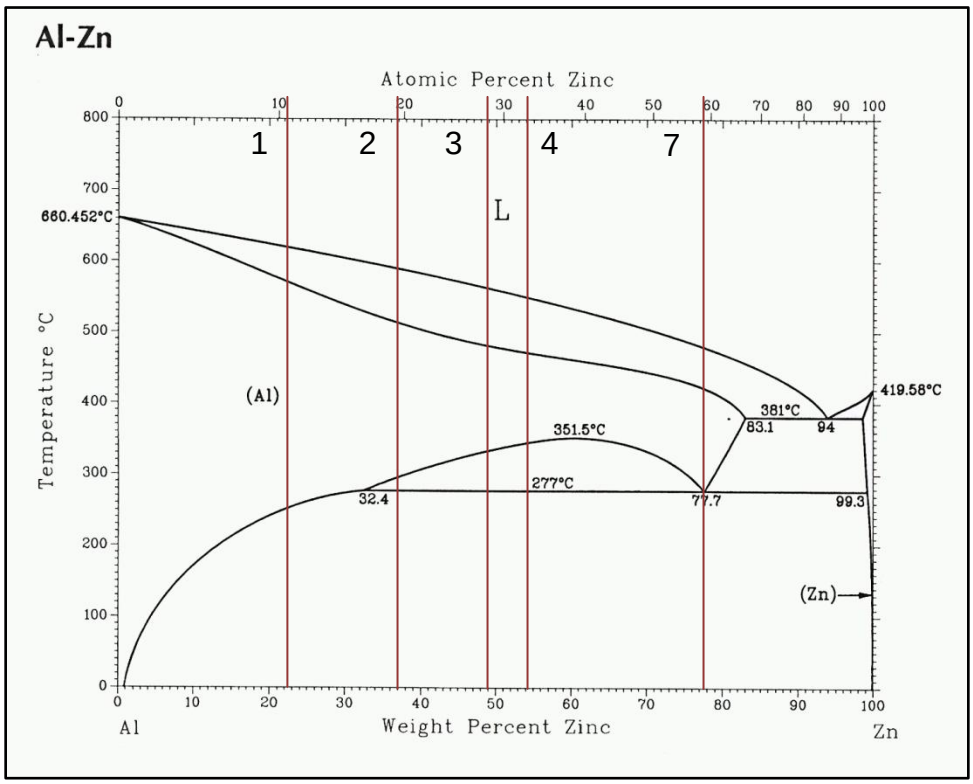

Figure 4.1 Al-Zn phase diagram. Vertical lines represent selected alloys to be dealloyed.

4.2 QUENCHING

As shown in the phase diagram in figure 4.1, zinc has a high solubility in aluminum. The typical Al-Zn binary alloy microstructure has aluminum-rich dendrites containing dissolved zinc, while zinc solid solution is present around the dendrite arms. Naturally, this non-homogeneous microstructure would directly affect the porosity obtained by chemical dealloying. If the corrosive media removes Zn atoms, nanoporosity evolution would only take place inside the aluminum rich areas while the rest of the porosity would be the result of pure Zn removal. On the other

hand, if the media attacks the aluminum phase, a Zn skeleton with big pores would result. Nanoporosity formation is favored when there is a complete homogeneous mixture between the two metallic elements. This microstructure can be achieved by adjusting the solidification rate.

Many binary systems have a natural tendency to create non-homogeneous microstructures mostly because of phase precipitation and microsegregation, which can be prevented or minimized by rapid cooling upon solidification. In this work, the use of different fast cooling rates helped increase the metastable retention of Zn atoms in the Al solid solution; this reduced the amount of zinc around the dendrites and ultimately formed a better microstructure with the potential to create nanoporosity in larger regions of the alloy sample.

In order to quantify the effect of cooling rate on the precursor alloy dendrite size, after quenching the microstructure of each treated specimen was studied. In figure 4.2 the resulting average secondary dendrite arm spacing (SDAS) for the different quenching techniques is shown. This measurement was used to quantify the approximate respective local solidification times. Figure 4.3 is a linear adjustment using logarithmic scales in which the solidification time can be found using SDAS. This chart is based on calculations made for aluminum 7075 alloy in which zinc is one of the mayor alloy elements.

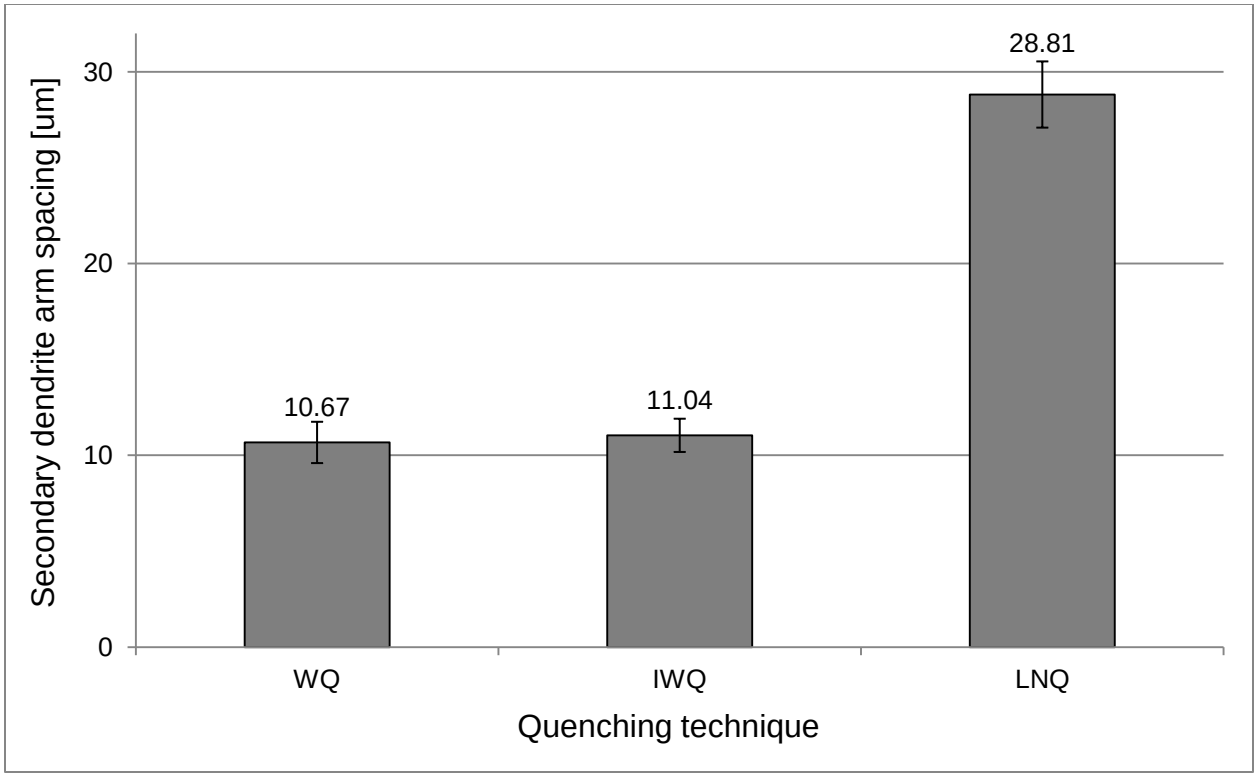

Figure 4.2 Average secondary dendrite arm spacing for the three cooling techniques.

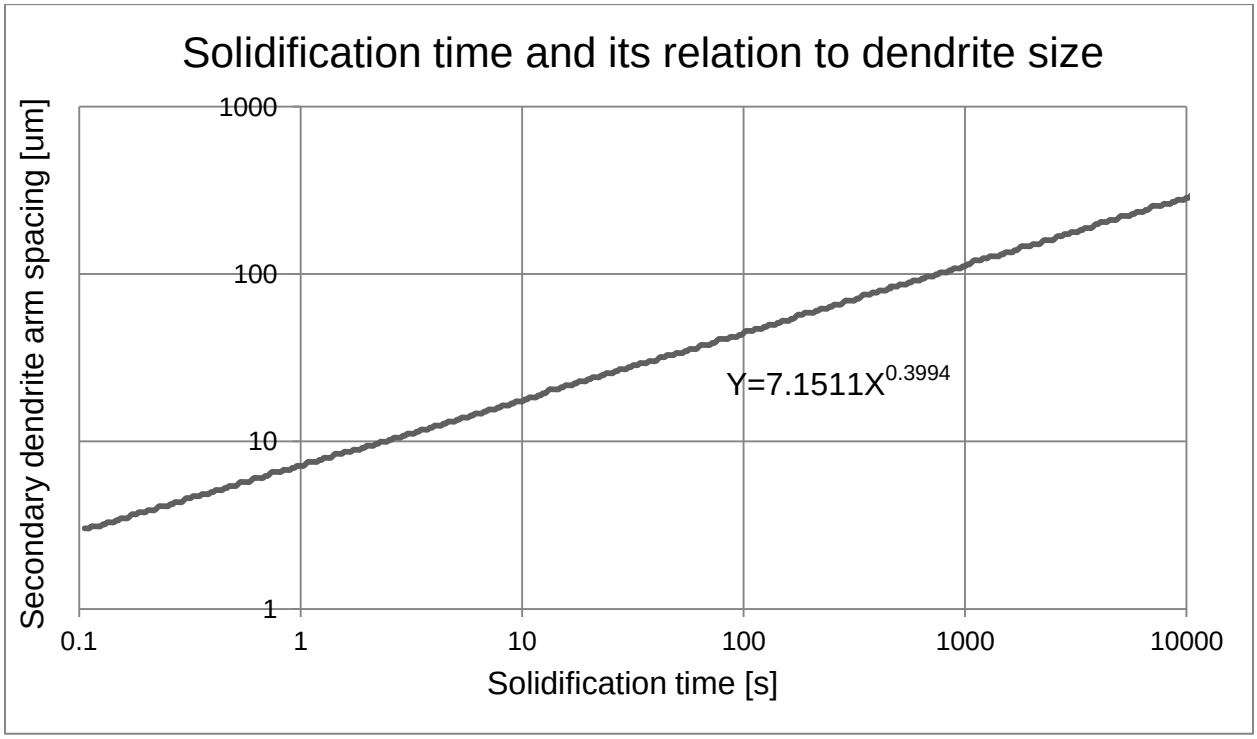

Figure 4.3 Solidification time and its relation to dendrite size [32].

The solidification times obtained from figure 4.3 were not as expected. Table 4.1 summarizes the solidification times for the three different cooling techniques employed in this thesis. We hypothesized a directly proportional relationship between solidification time and temperature of quenching media. The collected data seems to evince the contrary. There was a 30 second difference in solidification time between samples cooled with water at room temperature and those cooled with liquid nitrogen. The temperature difference between these cooling baths was very large; liquid nitrogen was 230˚C cooler than room temperature water. The aluminum phase appears to grow larger with lower temperatures. This is inconsistent with metallic crystal growth behavior.

Table 4.1 Rapid solidification techniques and their respective secondary dendrite arm spacing and solidification times.

Quench methods	SDAS [um]	Solidification time [s]
WQ	10.67	2.72
IWQ	11.04	2.96
LNQ	28.81	32.75

Two possible explanations can be used to justify this apparent incongruence. First, the amount of dissolved zinc inside the dendrite is so large that makes it a non-typical one, augmenting the arm size and ultimately invalidating the use of figure 4.37 to measure the solidification time. This explanation might appear inconsistent with the fact that the data shown in figure 4.3 is based on a 7075 alloy in which zinc is the primary alloy element. It is important to note that 7075 aluminum alloys only posses a maximum of 6 wt. % zinc; our least concentrated alloy had 30 wt. % zinc. The possibility of using this explanation to justify the incongruence comes up because of the observations taken when performing the quenching. Based on the SDAS measurements, the liquid nitrogen quenched samples solidify in 32.75 seconds. This does not correspond to the observed solidification time. It was noted that almost instantly, after pouring the melted sample in the liquid nitrogen bath, the sample was solid.

The second explanation can simply be that liquid nitrogen quenching is not as effective as expected. Pouring a 750˚C melted alloy in a cooling bath containing liquid nitrogen generates a large amount of gas. As a consequence, nitrogen bubbles are formed on the interface between the metal and the liquid. They might be creating a thermal barrier separating the quenching medium from the metallic sample. As stated before, the sample appeared to solidify instantly once submerged in the bath, making the comparison between observations and measurements inconsistent.

The increase in SDAS size was evident. A visual comparison between samples quenched with different processes revealed a completely different microstructure. Figure 4.4 is an optical micrograph of an Al-25 at. % Zn alloy quenched in water at room temperature. Small equiaxed dendrites are apparent. For this specimen, the measured mean SDAS was 10.67 μm. Moreover, figure 4.5 shows the same alloy in figure 4.4, but quenched in liquid nitrogen. For the specimen in this figure the average SDAS was 28.81 μm. Both figures, i.e. 4.4 and 4.5, were obtained with the same magnification and evinced that the cooling rate had a strong effect on the quenched microstructures, which then can affect the distribution of Zn in the samples.

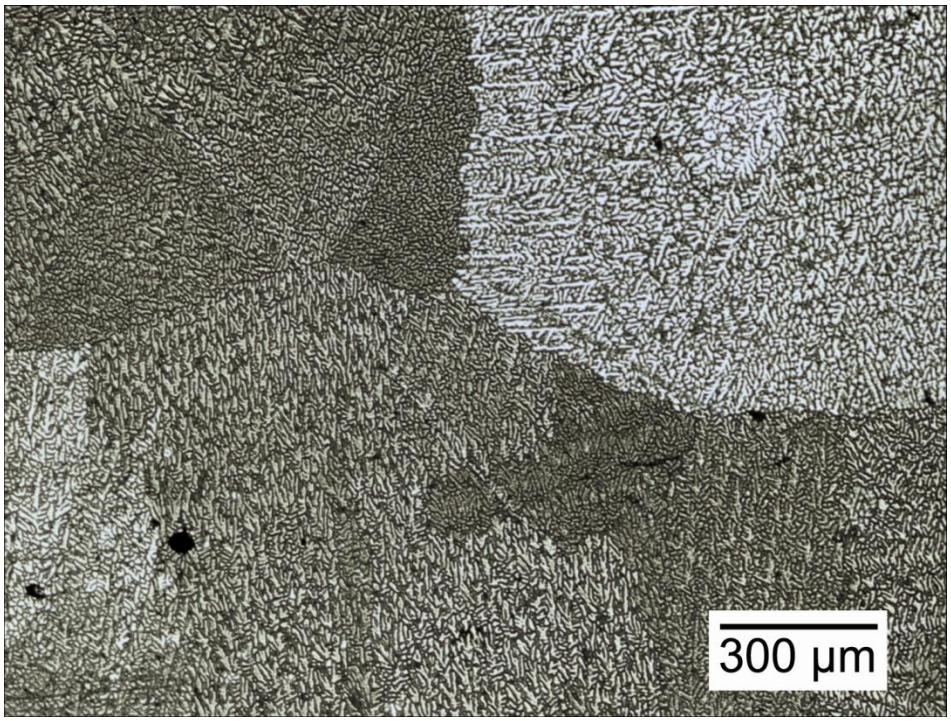

Figure 4.4 Optical microscopy image of Al-25 at. %Zn alloy quenched in water at room temperature. The sample was polished and etched for 5s with 10 wt. % NaOH.

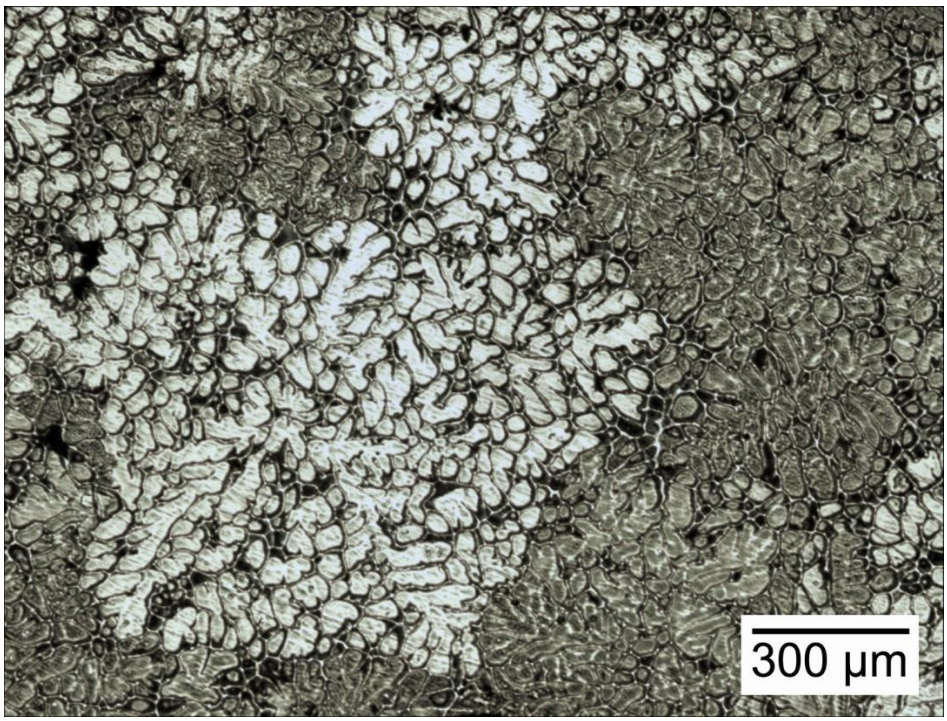

Figure 4.5 Optical microscopy image of Al-25 at. %Zn alloy quenched with liquid nitrogen. The sample was polished and etched with 10 wt. % NaOH solution.

4.3 CORROSION

As mentioned before, in order to create porous metal using Al-Zn alloys as precursor materials, a corrosive medium that removes only one of the species is needed. This medium can be of various types (aqueous solution, molten metal, gaseous, etc. [33]), for only a chemical reaction is needed between ions in the medium and the metal to be removed. For the present thesis, an aqueous solution was chosen based on several reasons. First, an aqueous solution was needed to apply potential in the electrochemical cell. Second, in almost every published work on chemical dealloying, aqueous solutions are used to remove the less noble specie and it was not the purpose of this thesis to study new methods of corrosion. Finally, inexpensive aqueous solutions can be readily prepared, while their concentration can be perfectly controlled. Scientists have used different solutions to create different porous metals but, since no one has ever worked on Al-Zn alloys, the right media was unknown to us. Additionally, we wanted to create two porous metals, zinc and aluminum. This dual objective suggested that two different solutions were needed.

A small experiment was conducted to select the corrosive media. Pure zinc and pure aluminum pellets were individually submerged in 20ml of two aqueous solutions to observe their effect on the metals. The sampled solutions were nitric acid (HNO_3) and sodium hydroxide (NaOH). These solutions were selected based on those mostly used in the literature. The concentrations of the solutions were also changed to observe its effect if any. Tables 4.2 and 4.3 summarize the results for aluminum and zinc respectively.

Table 4.2 Aluminum reactions to different aqueous solutions.

Concentration	NaOH	HNO_3
1 wt. %	Large amount of minute bubbles, fast corrosion	No visible change, no bubbles
25 wt. %	Very large amount of minute bubbles, very fast corrosion	Very small amount of bubbles after some time

Table 4.3 Zinc reactions to different aqueous solutions.

Concentration	NaOH	HNO_3
1 wt. %	Very small amount of bubbles, very slow corrosion	Very small initial amount of bubbles, amount of bubbles increases with time
25 wt. %	Very small amount of bubbles	Very large amount of big bubbles, very aggressive corrosion, zinc pellet is dissolved in less than 30s

As observed in the results gathered in Tables 4.2 and 4.3, aluminum was largely affected by the treatment with NaOH while zinc reacted vigorously in nitric acid. Selection of solution concentration was based on the reaction velocity. Even though the rate of corrosion was not measured for any of the solutions, a sense of difference in speed of corrosion was possible via optical inspection. It was observed that by increasing the concentration of HNO_3 the reaction of zinc was increased. If 20ml of 25 wt. % solution of HNO_3 was sufficient to completely dissolve the zinc pellet in less than 30 seconds, it was obvious to us that this solution was too concentrated. The process of dealloying depends on surface diffusion for its evolution and such fast and aggressive corrosion could impede this movement. Therefore, a 1 wt. % solution of HNO_3 in water was selected as the acidic corrosive medium after noting the increase in bubble formation in the more concentrated solution.

To select the solution to remove aluminum we followed the same procedure. HNO_3 did not affect aluminum as NaOH did. As soon as the pellet touched the NaOH solution, plenty of

bubbles started emerging from the surface of the metal. A difference in the amount of bubbles between 1 wt. % and 25 wt. % was observed. It was also observed that a longer period of time was needed for the pellet to be completely dissolved, and this was not affected by the concentration of the aqueous solution. For these reasons, a 25 wt. % solution of NaOH in water was selected for the removal of aluminum. This concentration was found to be relatively fast but not as aggressive to dissolve the pellet in seconds. Selecting an effective method of corrosion followed.

Generally there are two ways to apply the corrosion process in selective dissolution: the natural direct way of free corrosion and that of corrosion induced or helped by an applied electrical potential. Sections 4.2.1 and 4.2.2 will discussed both methods as they were applied in this work.

4.3.1 FREE CORROSION

Free corrosion involves only the submersion of the sample into the aqueous solution for a given period of time. Because this process is a relatively simple one, two factors can then be controlled: the temperature and time of corrosion.

Temperature normally increases corrosion rate. However, observations done with pure metals, as described in section 4.2, revealed already fast corrosion rates. Since the main objective of this thesis was to create porous zinc and porous aluminum while observing the effect of microstructure on final porosity, accelerating the rates was not needed. Temperature remained constant (room temperature) for all corrosion procedures.

Corrosion time can directly affect the final morphology and amount of porosity. It can be safely stated that this parameter has a linear relationship with the amount of less noble metal removed. Most researchers finish the free corrosion process until “no obvious bubbles emerge” [27]. This means that the corrosion is held until there is no more of the less noble metal available to be ionized or until the system reaches equilibrium.

There are cases where the corrosion process must be stopped before completion because some corrosive solutions can dissolve both metals in the alloy. Porous metals can be fabricated using these solutions, but the researcher must pay very close attention to the time of corrosion. If selective dissolution is attempted with a medium that dissolves both metals, the difference in potentials must be high enough such that the less noble metal dissolves first (galvanically). In the present work it was been found that NaOH dissolves both aluminum and zinc. It was observed that bubbles never cease to emerge, and after very long periods of

corrosion the entire sample was dissolved. For this reason, the free NaOH corrosion time selected was one hour. Sections 4.2.1.1 and 4.2.1.2 describe free corrosion for NaOH and HNO_3 respectively.

4.3.1.1 FREE CORROSION IN NaOH

Both aluminum and zinc dissolve in sodium hydroxide. While aluminum reacts readily in NaOH solution, zinc produces few bubbles at a slow pace. These bubbles correspond to the production of hydrogen when zinc oxide (ZnO) is formed. In other cases no gaseous hydrogen is generated as zinc hydroxide ($Zn(OH)_2$) becomes the main product of the reaction. In most cases, both reactions occur simultaneously partially passivating and corroding the metal. This is a complicated phenomenon and it will not be further discussed. Nevertheless, the selective removal of aluminum out of the alloy was achieved after one hour of free corrosion. The following represents the reaction of aluminum in NaOH.

$$2Al(s) + 2NaOH(aq) + 6H_2O \rightarrow 2Na^+(aq) + 2[Al(OH)_4]^- + 3H_2(g)$$

Tetrahydroxidoaluminate ($[Al(OH)_4]^-$) along with ionic sodium and hydrogen gas are products of this reaction. For our samples, this was a rather fast corrosion process with hydrogen gas bubbles formation as indicator. As stated before, free corrosion with NaOH was held for only one hour. This time period assured only the selective removal of aluminum on a representative outside layer of the sample. Figure 4.6 is an SEM image of an Al-15 at. % Zn alloy water-quenched at room temperature. This sample was free corroded with a 25 wt. % NaOH solution for one hour. The selective removal of aluminum is evident. The typical Al-Zn alloy

microstructure consists of aluminum-rich dendrites with zinc-rich regions surrounding them. After corrosion the aluminum rich dendrites are almost completely inexistent. An interconnected structure of zinc elongated fingers composes the resulting morphology. The presence of mostly zinc in this sample is further corroborated in section 4.3.1 using X-ray diffraction analysis.

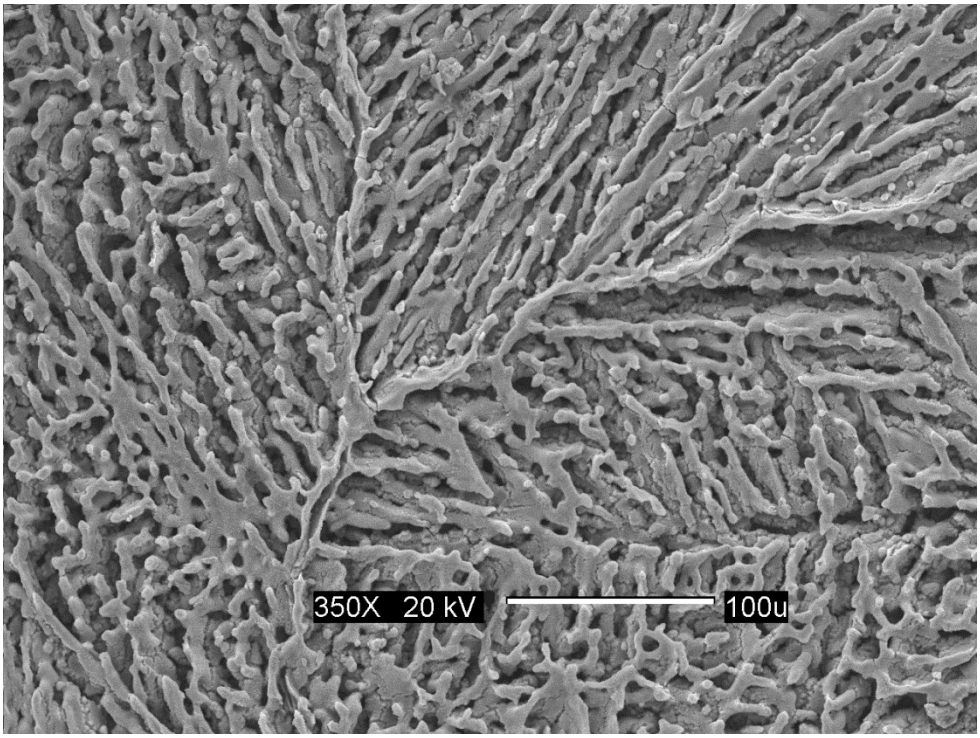

Figure 4.6 Al-15 at. % Zn quenched with water at room temperature, 25 wt. % NaOH free corroded for 1 hour. Notice aluminum-rich dendrite removal.

Increasing zinc concentration in the alloy decreased the amount of pores formed, as observed in figure 4.7. The sample, Al-40 at. % Zn free corroded in NaOH for 1 hour, presents traces of corrosion without any apparent porosity. One hour of free corrosion in 25 wt. % NaOH permitted porosity formation on concentrations up to 25 at. % zinc in aluminum. In figure 4.8

corrosion pits can be noticed and they seemed to be the precursor zones for pore formation. We believe that an increase in time of corrosion could result in pit growth and pore formation.

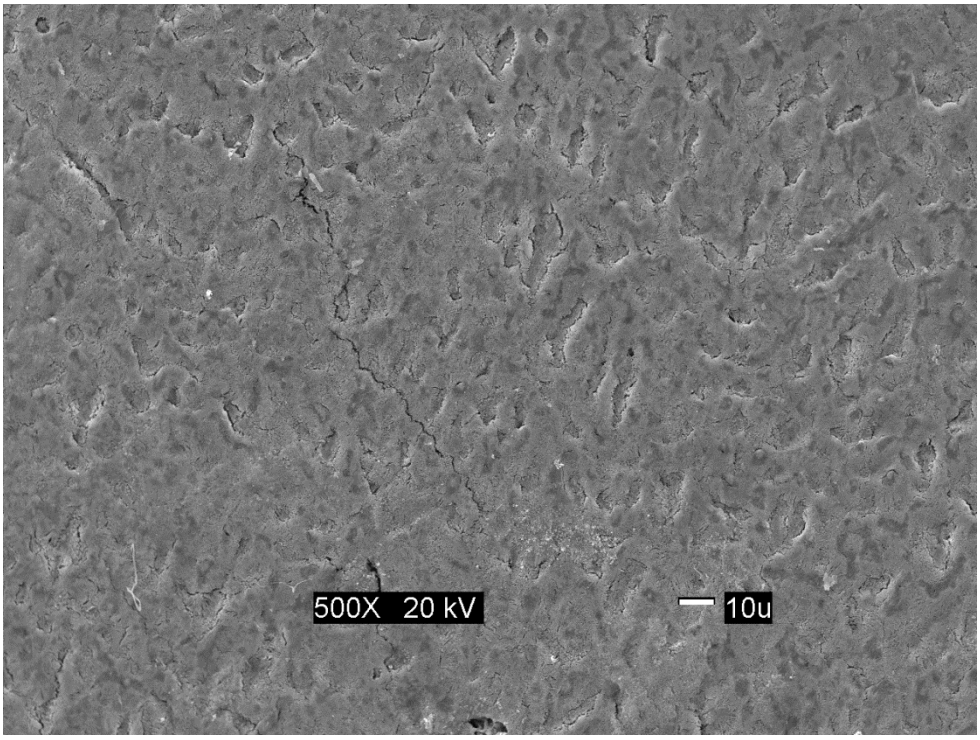

Figure 4.7 Al-40 at. % Zn quenched with water at room temperature, 25 wt. % NaOH free corroded for 1 hour. No apparent porosity formation.

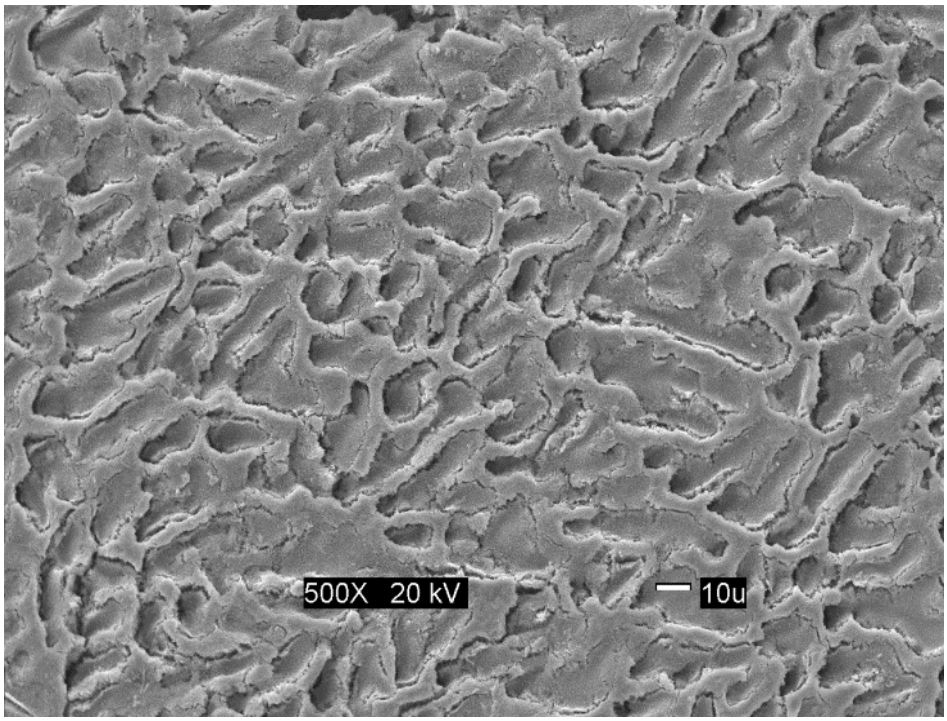

Figure 4.8 Al-25 at. % Zn quenched in water at room temperature and free corroded in 25 wt. % NaOH. Corrosion pits are evident. We believe they are precursor zones for pore formation

A different porosity was achieved when quenching at lower temperatures. Figure 4.9 shows a completely different porosity to that of figure 4.6. Peculiar geometrical shapes like pores are evident. No elongated, finger like ligament structure was found. The rapid cooling technique of iced water changed the way dendrites were formed and consequently the final porosity. Zinc rich dendrite boundary remained relatively untouched by the corrosive medium while aluminum rich dendrites where attacked.

Figure 4.9b revealed the selectiveness of the corrosive solution. Even thou the aluminum rich dendrites were readily attacked by the corrosion, the surrounding part of them seem less affected when compared to the inner area. White arrows point to the less affected sections. This finding reinforces the idea of high amounts of zinc dissolved into dendrites, and its relation to porosity formation.

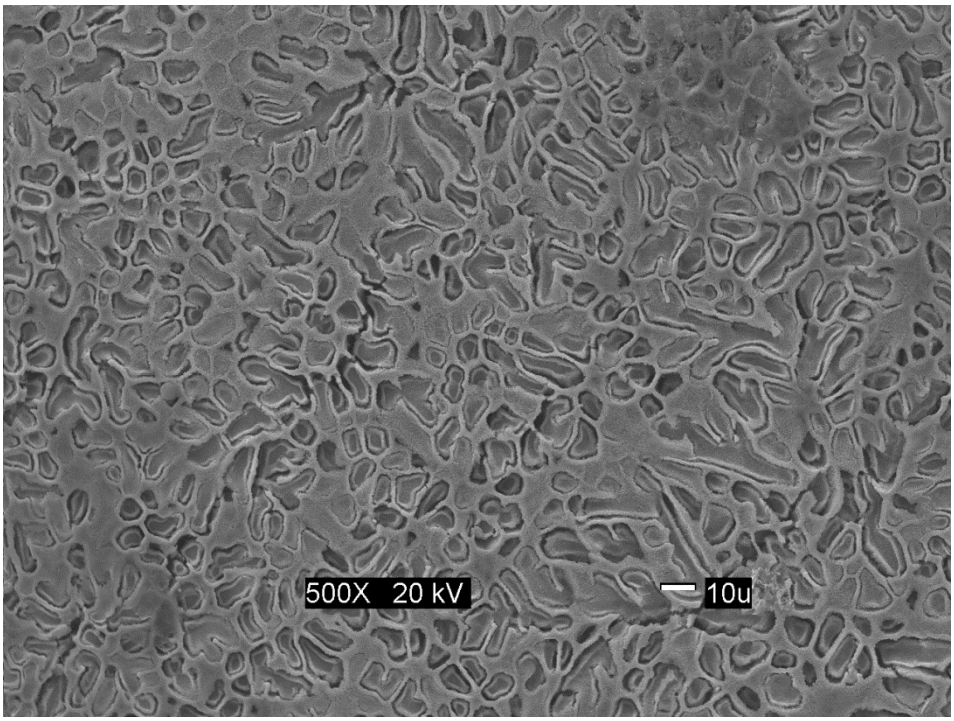

(a)

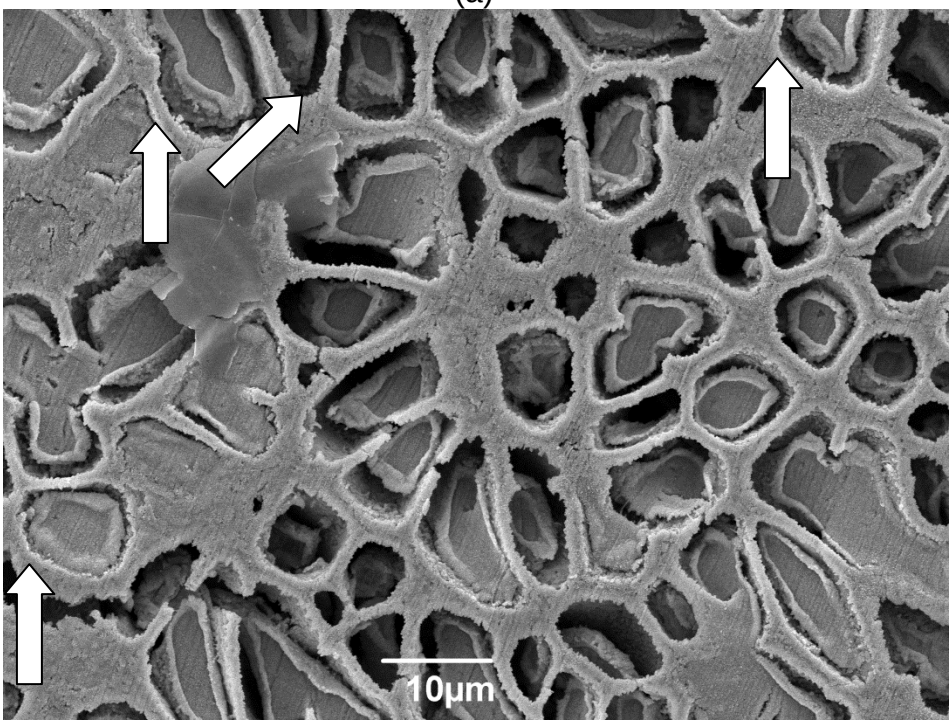

(b)

Figure 4.9 Al-35 at. % Zn alloy iced water quenched free corroded in 25 wt. % NaOH. a) No elongated, finger like ligament structure was found. Peculiar geometrical shapes are evident. b) Surrounding part of attacked dendrites seems less affected to corrosion. White arrows point to less affected sections.

Alloys with lower concentrations of zinc resulted with similar porosity but with thinner ligaments. Figure 4.10 and 4.11 are SEM micrographs of 25 and 15 atomic percent zinc alloys respectively. Disconnected zinc ligaments are observed with 25 at. % Zn while, almost complete loss of ligament connection is observed with less amounts of zinc.

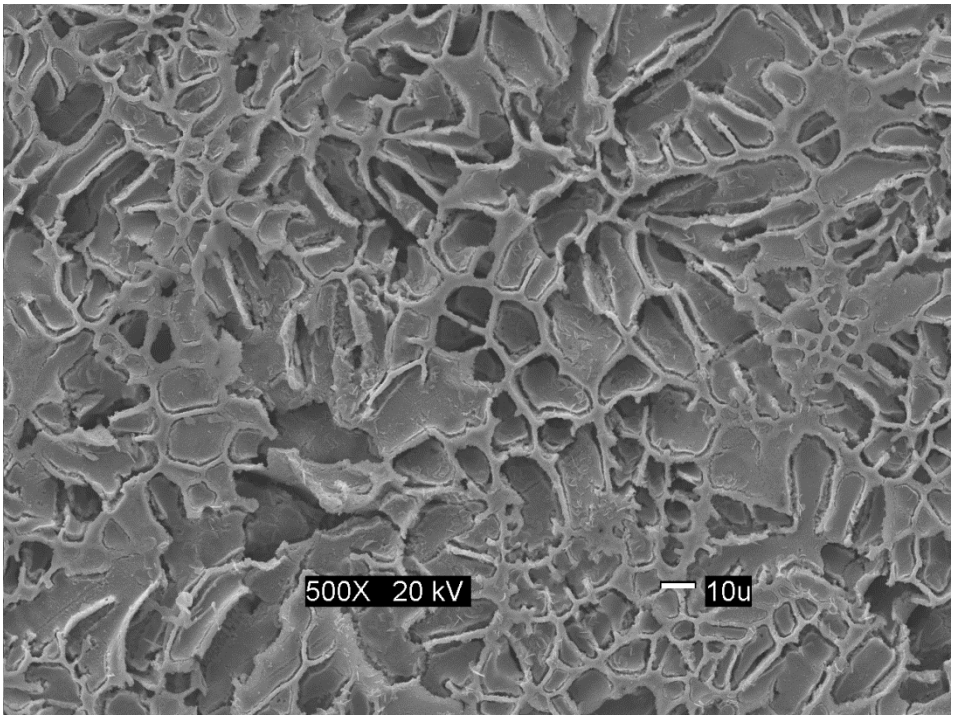

Figure 4.10 SEM image of an Al-25 at. % Zn alloy quenched in ice water and free corroded in NaOH. Disconected ligaments are evident.

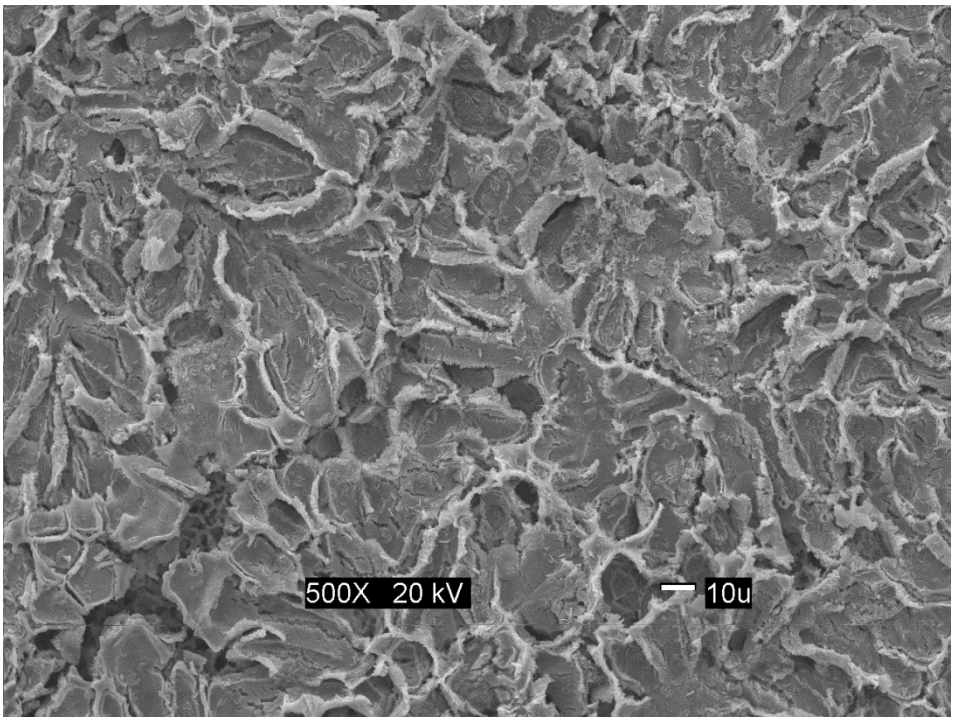

Figure 4.11 SEM image of an Al-15 at. % Zn alloy quenched in ice water and free corroded in NaOH. Small or null interconnection between ligaments is observed.

4.3.1.2 FREE CORROSION IN HNO_3

Aluminum and zinc react different in nitric acid: Aluminum passivates while zinc dissolves. The following is the chemical reaction involving the dissolution of zinc in HNO_3.

$$Zn(s) + 2HNO_3(aq) \rightarrow Zn(NO_3)_2(aq) + H_2(g)$$

The products of this reaction are zinc nitrate ($Zn(NO_3)_2$) and hydrogen gas (H_2), which. is the visual indicator of the reaction (bubbles). Zinc nitrate is in the aqueous form and it is not perceivable with the eye. Figure 4.12 shows an SEM micrograph of an Al-15 at. % Zn alloy free corroded in 1 wt. % nitric acid. Passivated aluminum dendrites surrounded by hollow regions are evident. These regions once where full of zinc. The selective dissolution of zinc by nitric acid is obvious. One might be tempted to think that all the zinc has been removed from the alloy, but further investigation revealed that some zinc was still present (trapped) in the aluminum rich areas. In section 5.2 an EDS analysis allows determining the presence of zinc after nitric acid corrosion.

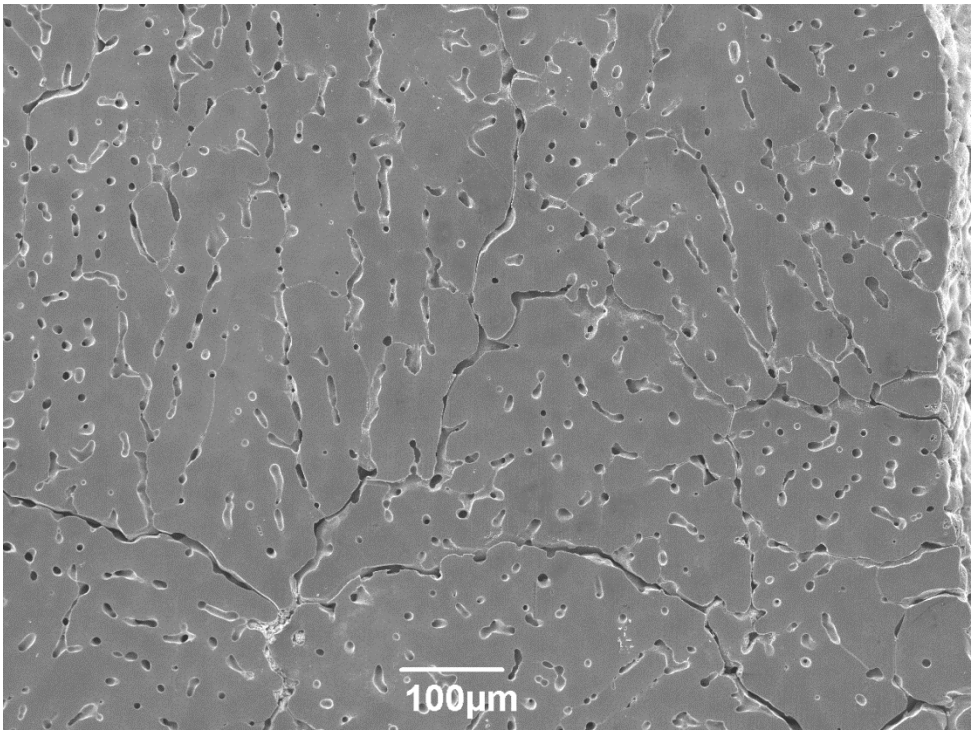

Figure 4.12 Al-15 at. % Zn alloy quenched in nitric acid and free corroded in 1 wt. % HNO_3. Zinc has been selectively dissolved and aluminum passivated by the acid to create a porous structure.

Figure 4.13 further evince the removal of zinc by nitric acid under free corrosion conditions. In figure 4.13a, black arrows point at passivated aluminum rich areas. The aluminum in these areas has reacted with HNO_3 to produce a thin layer of aluminum oxide (Al_2O_3). This oxide film functions as a barrier against ions and impedes further corrosion. The white circle indicates regions before filled with zinc. This precise corrosion and removal of metal provides the foundation of selective dissolution. Only the less noble metal (in this case zinc) was removed.

A characteristic morphology in the walls of passivated aluminum rich dendrites was observed. These areas, once the interface between aluminum and zinc, now seem shallowly perforated and scratched. In figure 4.13b this morphology is evident.

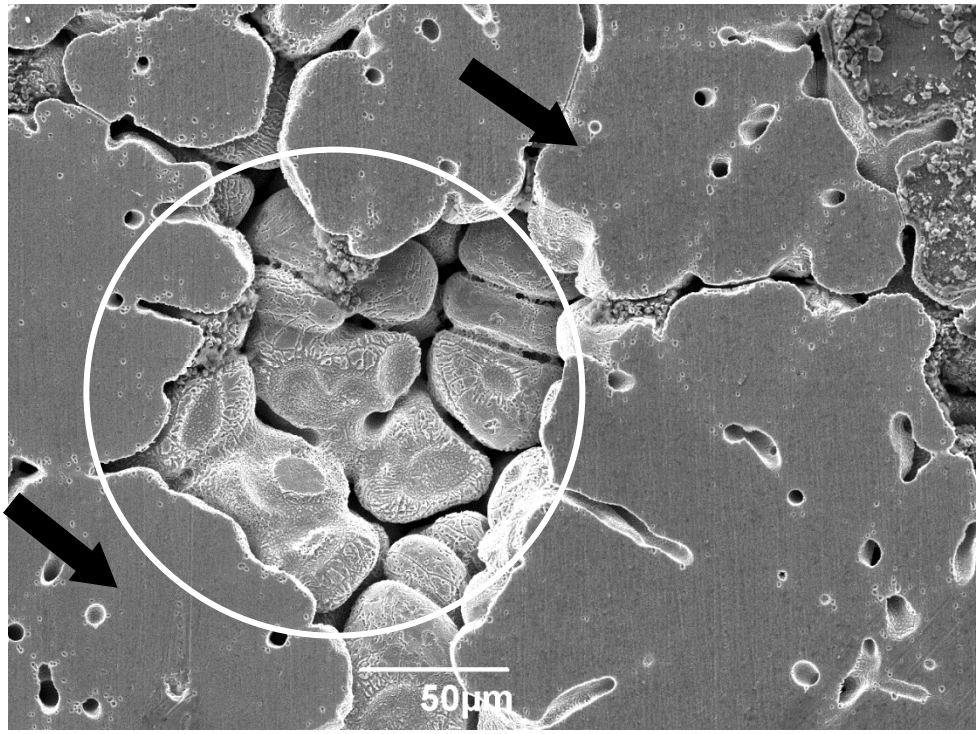

(a)

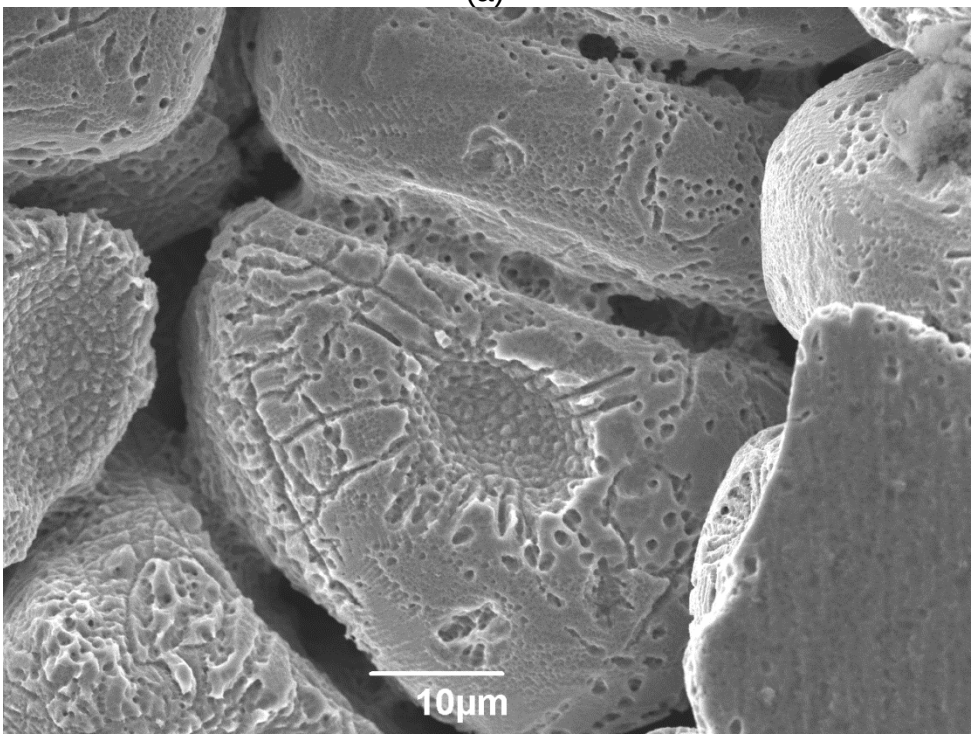

(b)

Figure 4.13 Al-15 at. % Zn alloy quenched in nitric acid and free corroded in 1 wt. % HNO3. a) Black arrows indicate passivated aluminum regions. b) Magnification of encircled region.

The formation of dimples along the surface was a result of the selective removal of zinc. In our quenched samples, the interface between aluminum rich dendrites and zinc rich boundaries is a region of solid solution. Zinc is generally located in two regions; the zinc rich phase acting as boundary separating dendrites and the outer sections of dendrites. Great amount of zinc was dissolved in the outer layers of the dendrites. An EDS analysis before corrosion evinced the high concentration of zinc in the outer parts of the dendrites. These results will be discussed in section 5.2.

After the fast removal of zinc from the boundaries, the ions in the medium would move to the next zinc rich region: the dendrite outer layer. The process of dimple formation might be the result of a physical race between the growing aluminum oxide films and zinc nitrite being dissolved into solution.

Figure 4.14 shows a typical dimpled surface of a dendrite wall after free corrosion with HNO_3. This morphology was not only present in the inner walls of the dendrites but also on the outer regions of the dendrites in polished face of the sample. Figure 4.15 perfectly presents the dimple formation around the dendrites. It can be observed how the dimples surround the dendrite finger. This face can represent a section view of a typical corroded dendrite. The restricted appearance of the dimples around the dendrites evinces their direct relation with amount of dissolved zinc. As one moves inside the dendrite and away from the boundary, the amount of zinc decreases.

This dimple formation in solid solution regions can be traces of first steps of nanoporosity evolution. The hypothesis is that in these solid solution regions, some aluminum atoms move on the surface to permit the dissolution of zinc. These aluminum atoms are then stopped by passivation, stopping also the evolution.

In figure 4.16 the morphology of the dimples can be appreciated. The dimples have an inverted pyramid shape. They do not seem to be organized in a specific pattern but rather are scattered and disorganized. Many different sizes of dimples are also observed. This difference in sizes can be the product of differences in corrosion-passivation-evolution dynamics. Various mechanisms might be interacting during the formation of the dimples. Surface diffusion of aluminum atoms, ionization and dissolution of zinc atoms, passivation and formation of aluminum oxides might occur at different rates resulting in different dimple sizes. Dimple formation would later become key to the formation of nanopores as alloy concentration increased and the corrosion mechanism was changed with an electric potential.

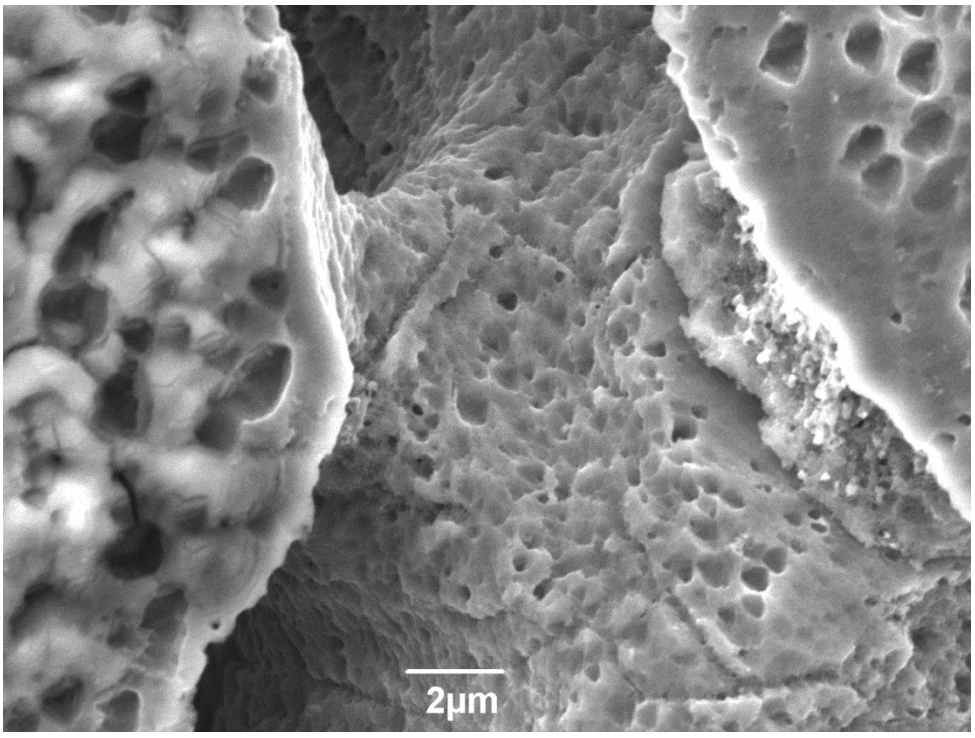

Figure 4.14 Al-15 at. % Zn alloy free corroded in 1 wt. % HNO_3. Typical dimpled surface of a dendrite wall after free corrosion.

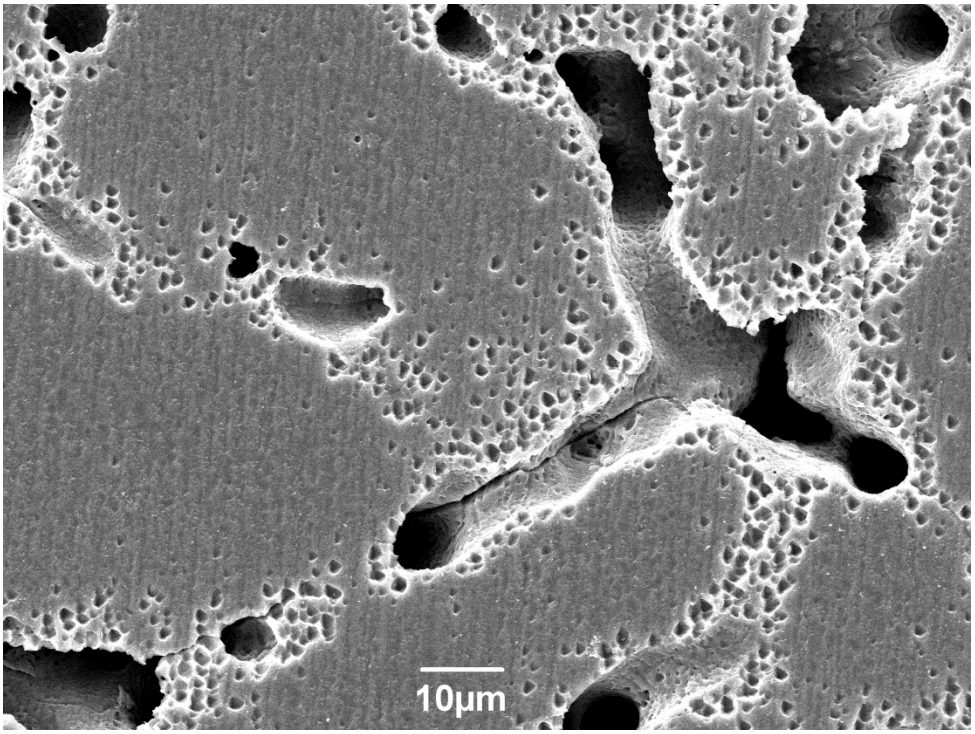

Figure 4.15 Al-25 at. % Zn alloy free corroded in 1 wt. % HNO_3. Dimple formation around dendrites.

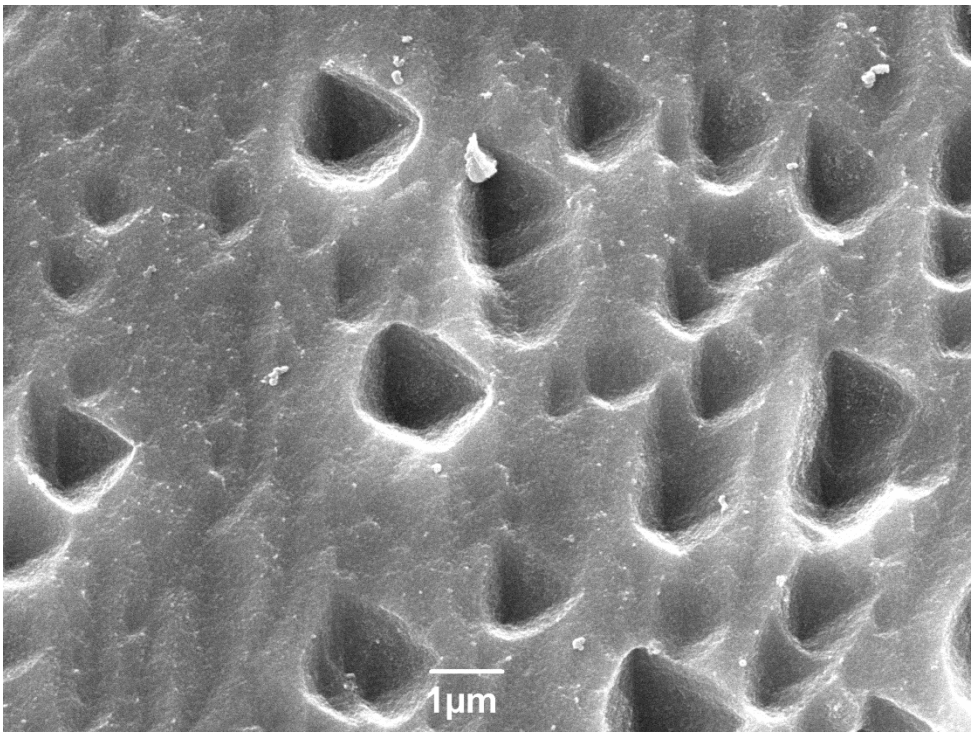

Figure 4.16 Al-25 at. % Zn alloy free corroded in 1 wt. % HNO_3. Pyramid like shape dimples on the polish surface.

Free corroding Al-Zn alloys in 1 wt. % HNO_3 solution produces porous aluminum alloys. When comparing pores with image scales an approximated pore size can be measured. The pore diameters are not smaller than 5μm. No nanoporous morphology was found using nitric acid under free corrosion for any of the alloy concentrations. The application of electrical potential provided the energy needed to produce smaller pores, especially on the aluminum rich regions. Next section will discuss the process here called “electrochemical corrosion”.

4.3.2 ELECTROCHEMICAL CORROSION

Technically, every metallic corrosion process in electrolytes is an electrochemical phenomenon because of the interchange of electrons. In this thesis, the term electrochemical corrosion refers to corrosion with an applied electric potential. A voltage was applied to the sample to help promote the dissolution of the less noble atoms. This voltage was held constant throughout the process. Although the amount of applied potential can affect the rate of corrosion [34], observing this effect was not one of our objectives. Instead, electric potential was used in an attempt to extend the nanoporosity evolution process while decreasing the passivation of the more noble metal.

4.3.2.1 ELECTROCHEMICAL CORROSION IN NaOH

The chemical reactions taking place in electrochemical corrosion are equal to those in free corrosion. Again, both aluminum and zinc dissolve in NaOH, but at different rates. Here aluminum is the less noble metal as the potentials provide for its galvanic dissolution.

Figure 4.17 shows a SEM micrograph of an Al-15 at. % Zn alloy electrochemically corroded in NaOH. This alloy shares the same zinc concentration, same cooling rate and same electrolyte medium as that in figure 4.6. The only difference between these samples was the applied potential. Compared to the one in figure 4.6 this alloy possesses a completely different morphology. Naturally the applied potential affected the final porosity. No finger-like ligament

exists and is replaced by an disorganized microstructure consisting of interconnected zinc and hollow spaces. It is difficult to identify the original dendrites and their boundaries. Changing the concentration of zinc in the alloy and quenching at lower temperatures increased the disorganization of the ligament network.

Figure 4.18 evinces the random porosity and ligament interconnection of an Al-35 at. % Zn alloy quenched in liquid nitrogen and electrochemically corroded in NaOH. It is almost impossible to identify the original dendrites or dendrite boundaries. The once organized, finger-like zinc ligaments turned into clusters of tiny zinc particles forming columns and walls. The applied potential increased the removal of aluminum while provided some energy for zinc atoms to reorganize.

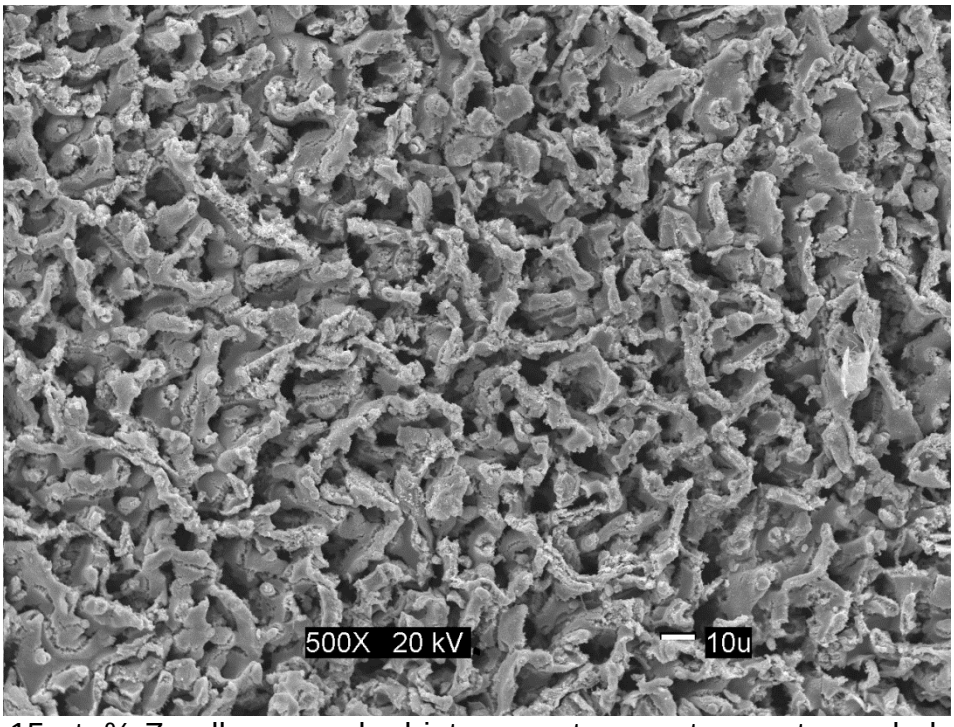

Figure 4.17 Al-15 at. % Zn alloy quenched into room temperature water and electrochemically corroded in 25 wt. % NaOH. Applied potential affected the final porosity. No finger-like ligaments. Disorganized microstructure of interconnected zinc.

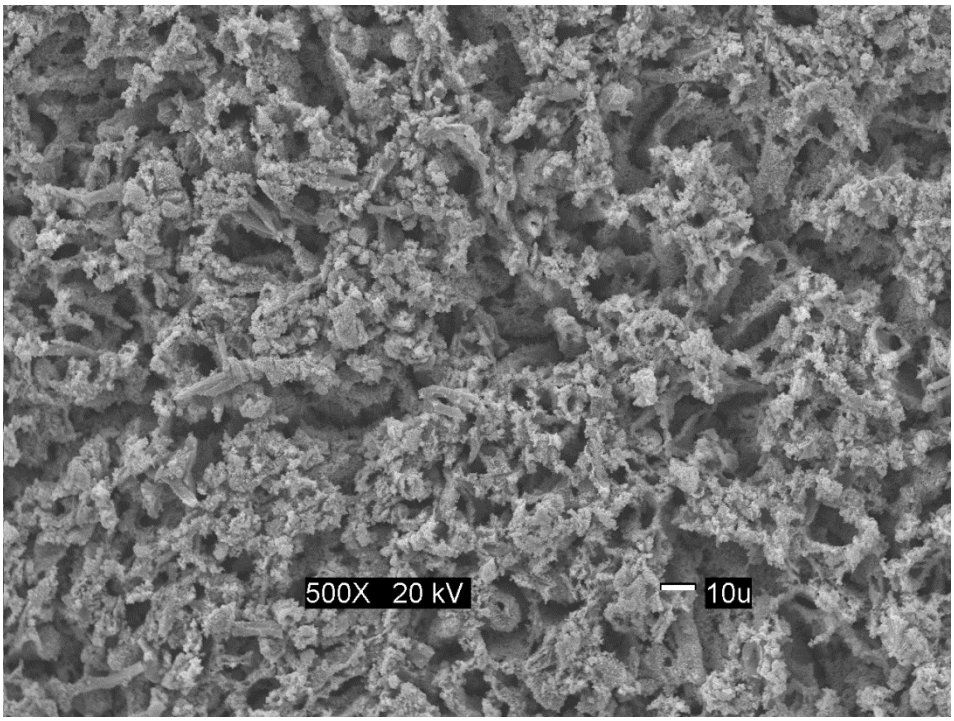

Figure 4.18 Al-35 at. % Zn alloy quenched into liquid nitrogen and electrochemically corroded in NaOH. Random porosity and ligament interconnection is evident. Original dendrites and dendrite boundaries are almost impossible to identify.

4.3.2.2 ELECTROCHEMICAL CORROSION IN HNO_3

As stated before, nitric acid removes the zinc out of the Al-Zn alloys. The selective dissolution of zinc in electrochemical corrosion with HNO_3 resulted similar to that of free corrosion. Selective removal of zinc was evident while passivation of aluminum remained. Figure 4.19 shows an Al-35at%Zn alloy electrochemically corroded in HNO_3. Dendrites are easily identifiable. Pockets of passivated aluminum-rich areas create an interconnected ligament network. Big pores are initially perceived but a closer observation reveals a secondary porosity with smaller diameter pores. This secondary porosity is concentrated inside dendrite islands and

appears to be resulting from the applied potential, as no secondary porosity was observed when no potential was applied.

In figures 4.20 and 4.21 this smaller secondary porosity is more visible. Based on the image scale, the pore diameters are less than 1μm. These pores seem to be interconnected and they can be found in all parts of the dendrite islands with a larger amount on the outer layers. It is believed that the large amount of secondary porosity around the outer layers of dendrites is directly related to dimple formation described in section 4.2.1.2. It is believed that the applied potential extended the dimple growth to the extent of porosity formation. These deep dimples, now pores, could have then become interconnected after the growth of neighbor dimples.

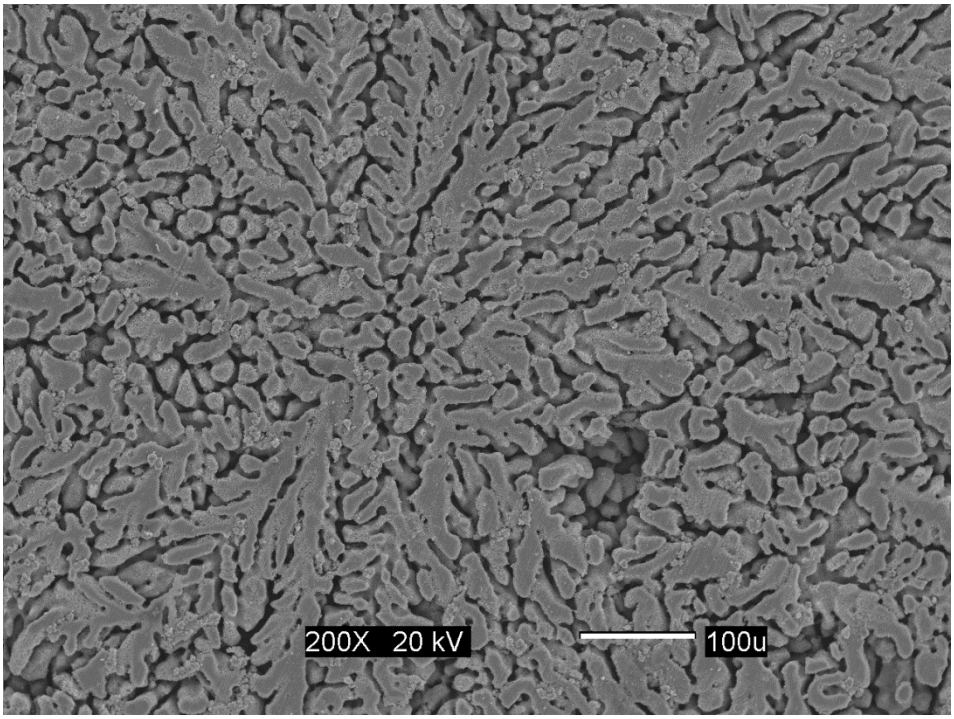

Figure 4.19 Al-35 at. % Zn alloy quenched into liquid nitrogen and electrochemically corroded in HNO_3. Pockets of passivated aluminum-rich dendrites create an interconnected network.

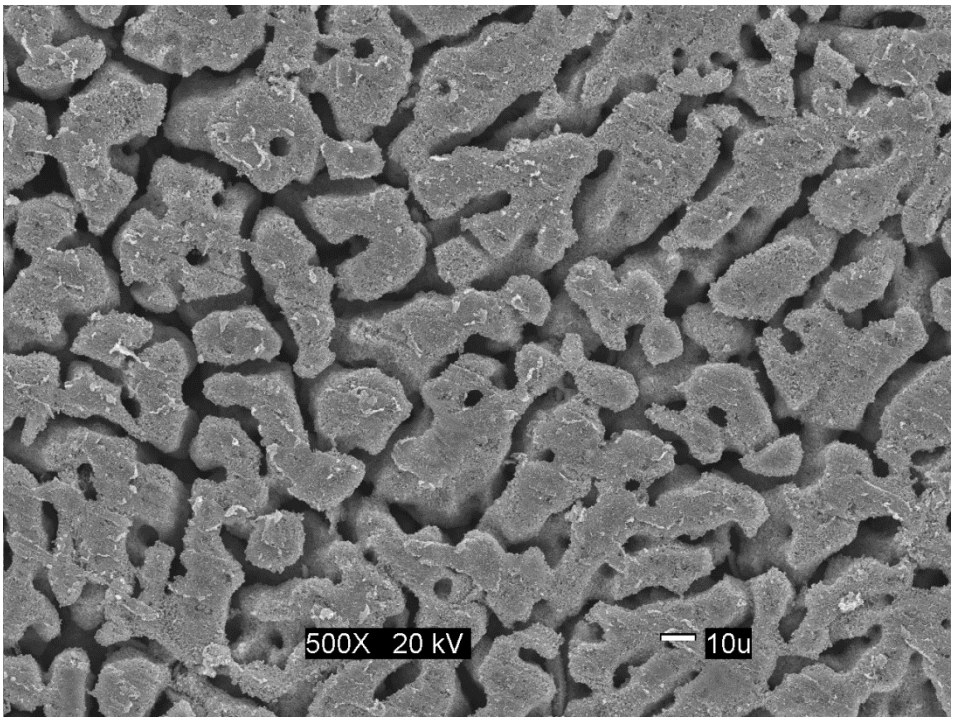

Figure 4.20 Al-35 at. % Zn alloy quenched into liquid nitrogen and electrochemically corroded in HNO_3.

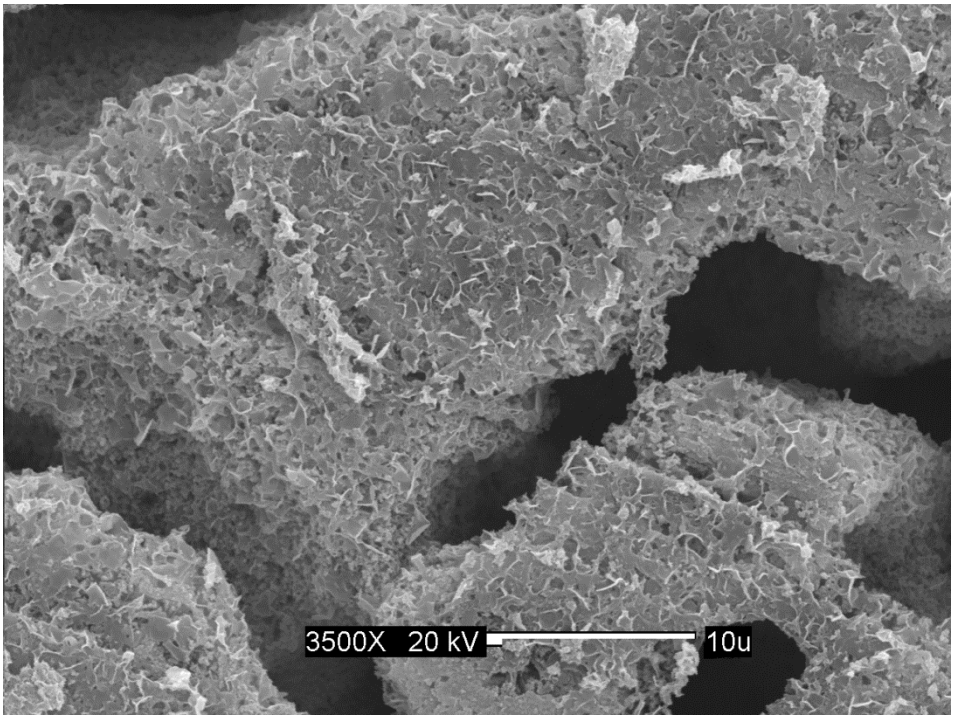

Figure 4.21 Al-35 at. % Zn alloy quenched into liquid nitrogen and electrochemically corroded in HNO_3. Smaller porosity concentrated inside dendrite islands.

Since dimple porosity is directly related to zinc concentration inside aluminum-rich dendrites, secondary porosity was observed in alloys with zinc concentration around 25 to 35 atomic percent. Figure 4.22 shows an Al-25 at. % Zn alloy rapidly cooled in liquid nitrogen and electrochemically corroded in HNO_3. The micrograph is similar to that of figure 4.20 with aluminum-rich dendrites separated by hollow regions once filled with zinc. The major difference between these samples is the apparent lack of secondary porosity in figure 4.22. Nonetheless, a closer inspection would evince the contrary.

Figures 4.23 and 4.24 show the same alloy with increasing magnifications. Secondary porosity is again evident but this time completely restricted to the outer regions of the dendrites. No secondary porosity can be seen inside dendrites. This finding further evinces the relationship between zinc concentration and porosity. Therefore, it is suggested that the cooling rate and concentration combination was not enough to successfully diffuse zinc in the dendrites, thus the lacking of secondary porosity inside. It was found that in order to promote the dissolution of zinc in aluminum, faster cooling rates were needed for less concentrated alloys. Another discovery revealed by these images was that porosity interconnection not only depends on dealloying, but also on how the dendrites grow.

As seen in figures 4.23, 4.24 and 4.25, when two dendrites are close enough, a different type of pore interconnection is created; thus further increasing the surface area of the porous sample. These new interconnected pores are created by neighboring dendrites sharing a common outer porous layer. The existence of this interconnection is not restricted to a few isolated regions but rather extends to all sections where very close neighbor dendrites exist.

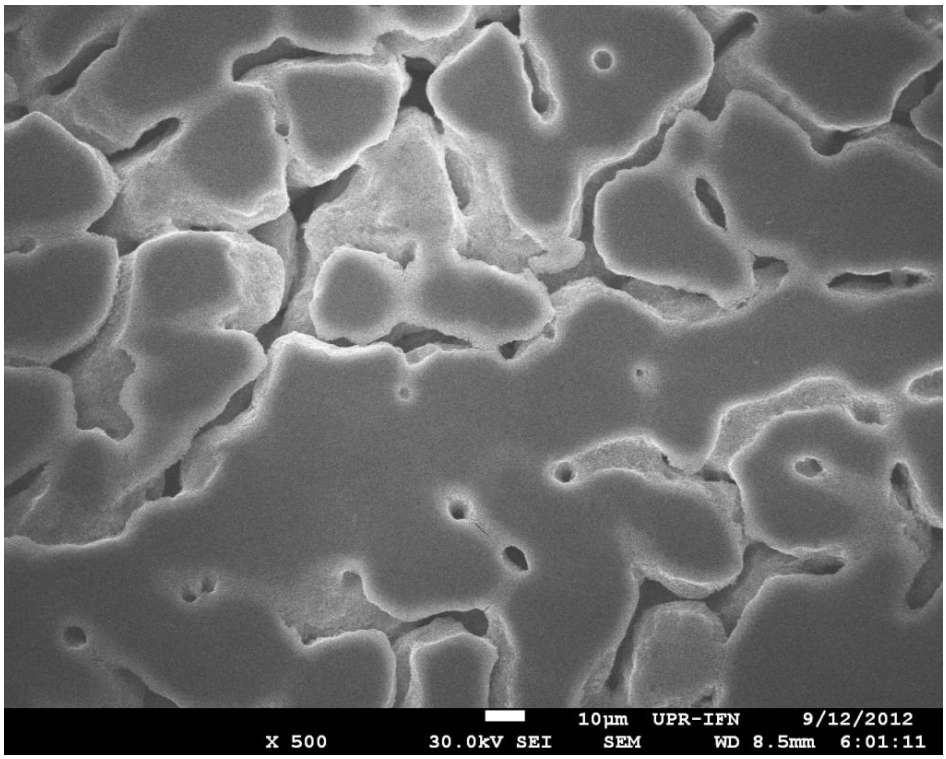

Figure 4.22 Al-25 at. % Zn alloy liquid nitrogen quenched and electrochemically corroded in HNO_3. Secondary porosity is restricted to the outer regions of dendrites. No secondary porosity can be seen inside dendrites.

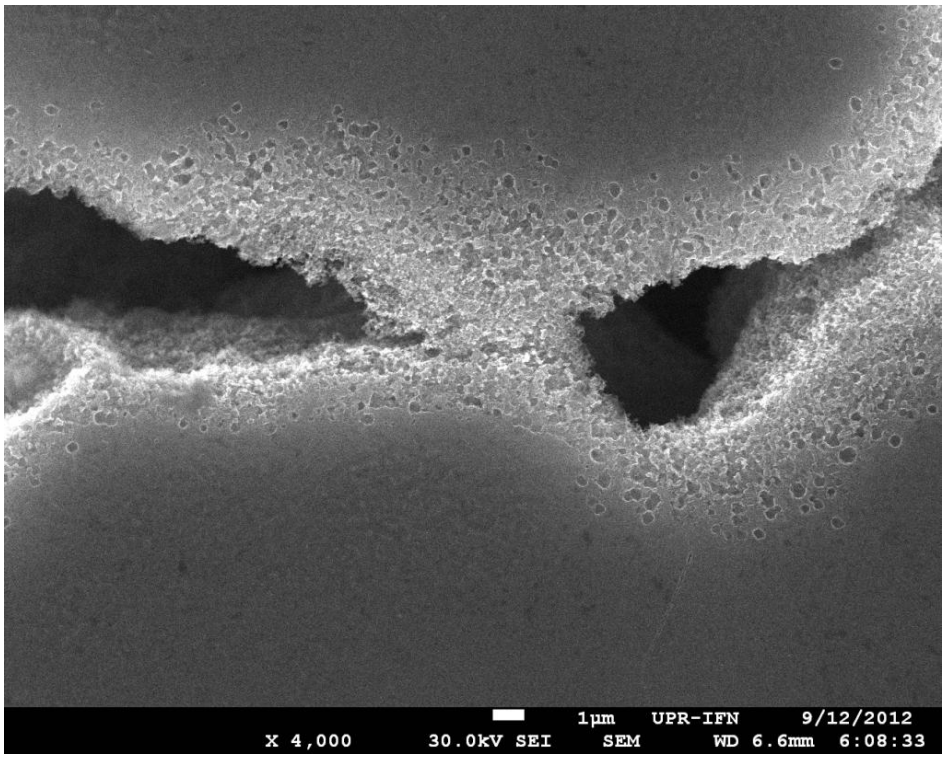

Figure 4.23 Al-25 at. % Zn alloy quenched into liquid nitrogen and electrochemically corroded in HNO_3.

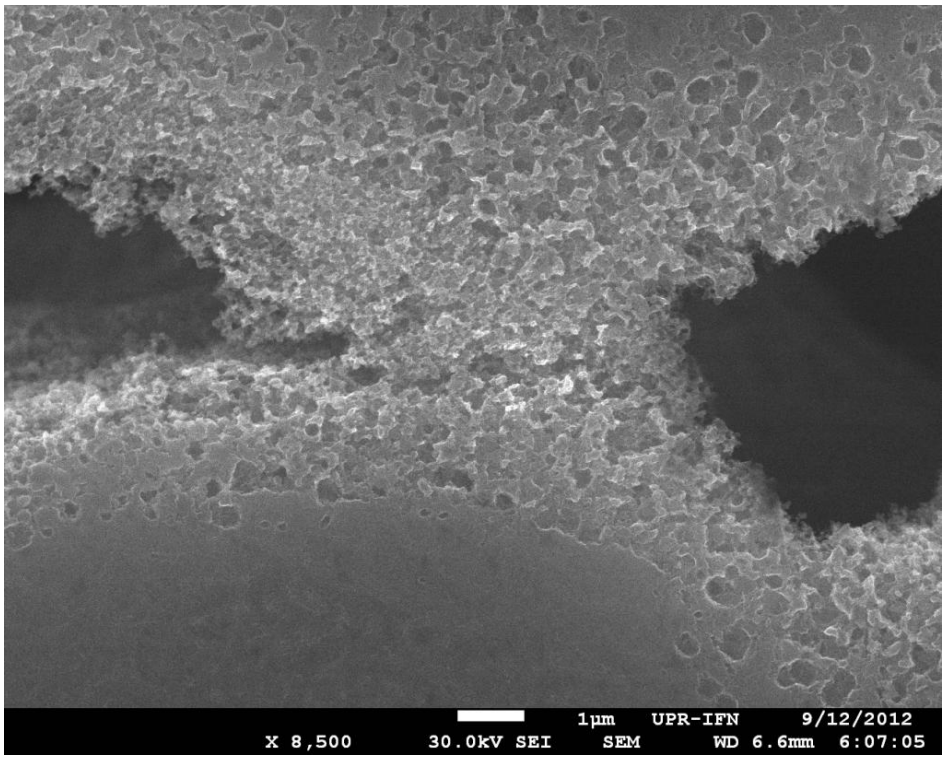

Figure 4.24 Al-25 at. % Zn alloy quenched into liquid nitrogen and electrochemically corroded in HNO_3. Neighboring dendrites sharing a common outer porous layer.

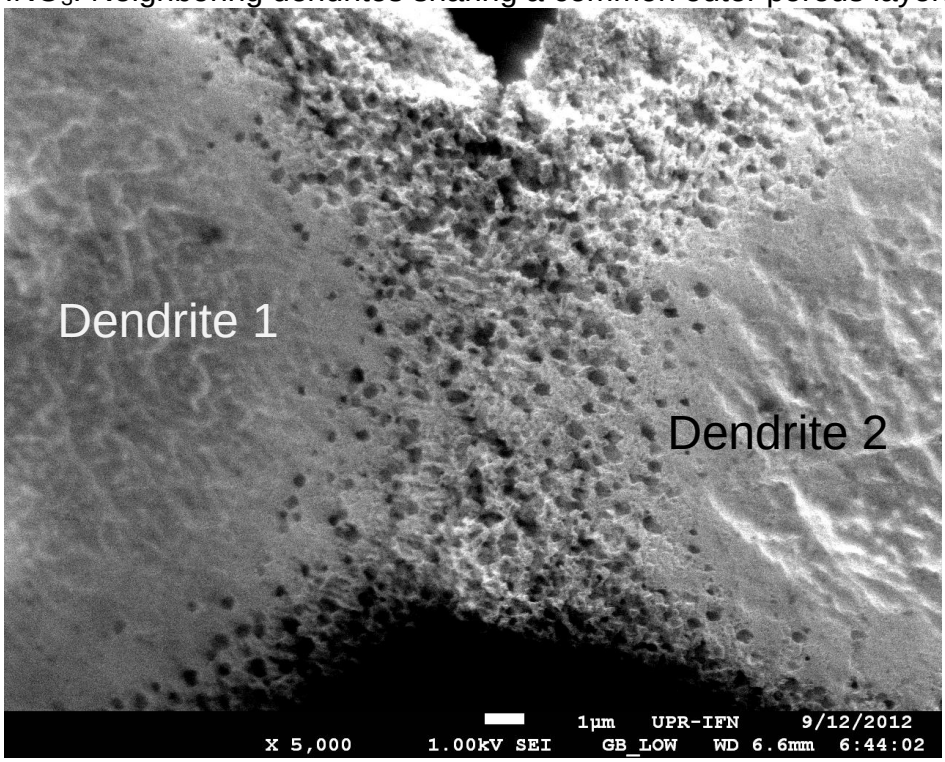

Figure 4.25 Al-25 at. % Zn alloy quenched into liquid nitrogen and electrochemically corroded in HNO_3. Very close neighbor dendrites results with high porous morphology.

Canyons (deep depressions) carved by dealloying resulted with very porous walls. The black circle in figure 4.26 shows a typical porous wall. A very rough and porous surface is evident. The pore depths are limited by the amount of zinc dissolved in the outer part regions of the aluminum-rich dendrite. Figures 4.27, 4.28 and 4.29 are magnified micrographs of the wall circled in figure 4.26. Small interconnected pores are apparent. Comparing pore diameters with scales in images 4.28 and 4.29 it is evident that many pores have less than 100 nm diameter. The combination of fast cooling rates and high zinc concentrations yield nanoporosity when electrochemically corroded in HNO_3.

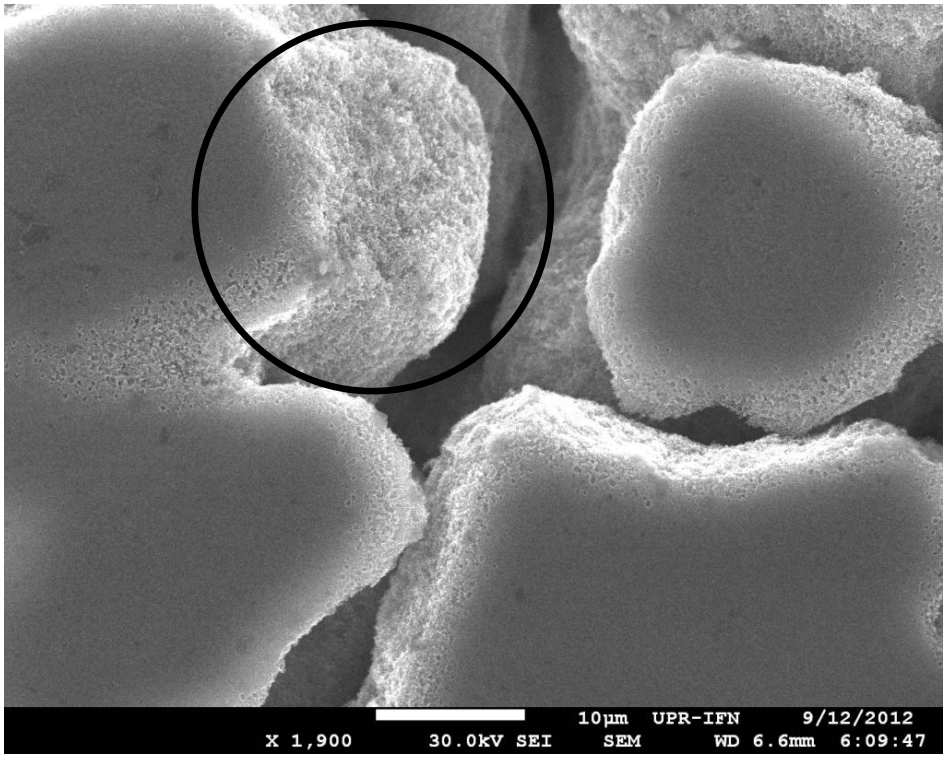

Figure 4.26 Al-25 at. % Zn alloy quenched into liquid nitrogen and electrochemically corroded in HNO_3. Black circle shows a typical rough and porous wall.

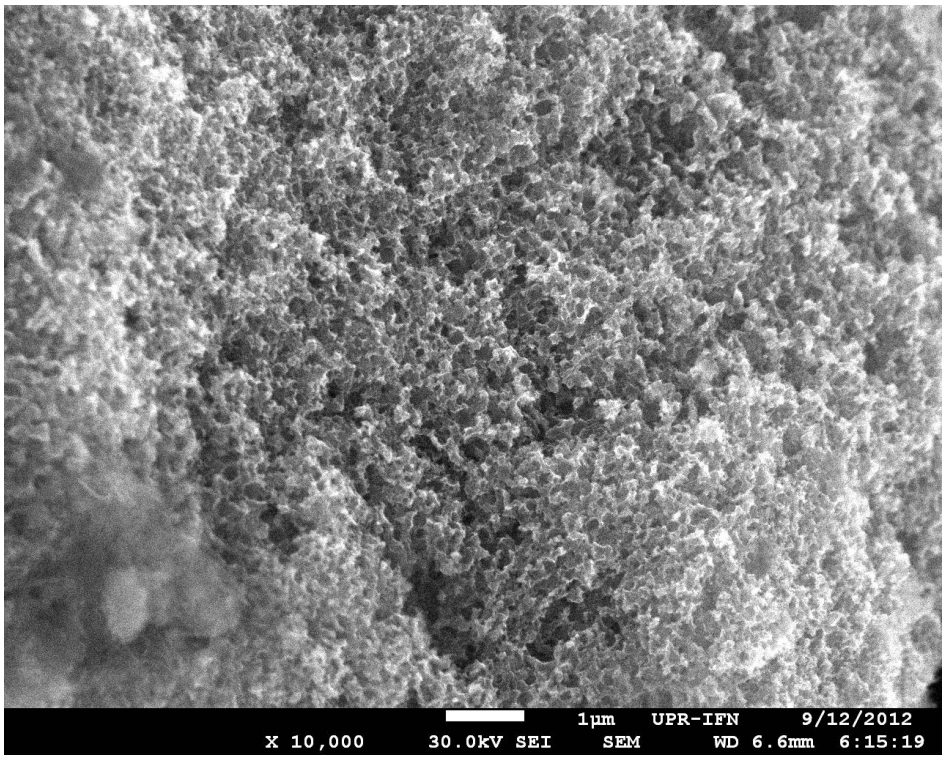

Figure 4.27 Al-25 at. % Zn alloy quenched into liquid nitrogen and electrochemically corroded in HNO_3. Magnification of black circle in figure 4.26.

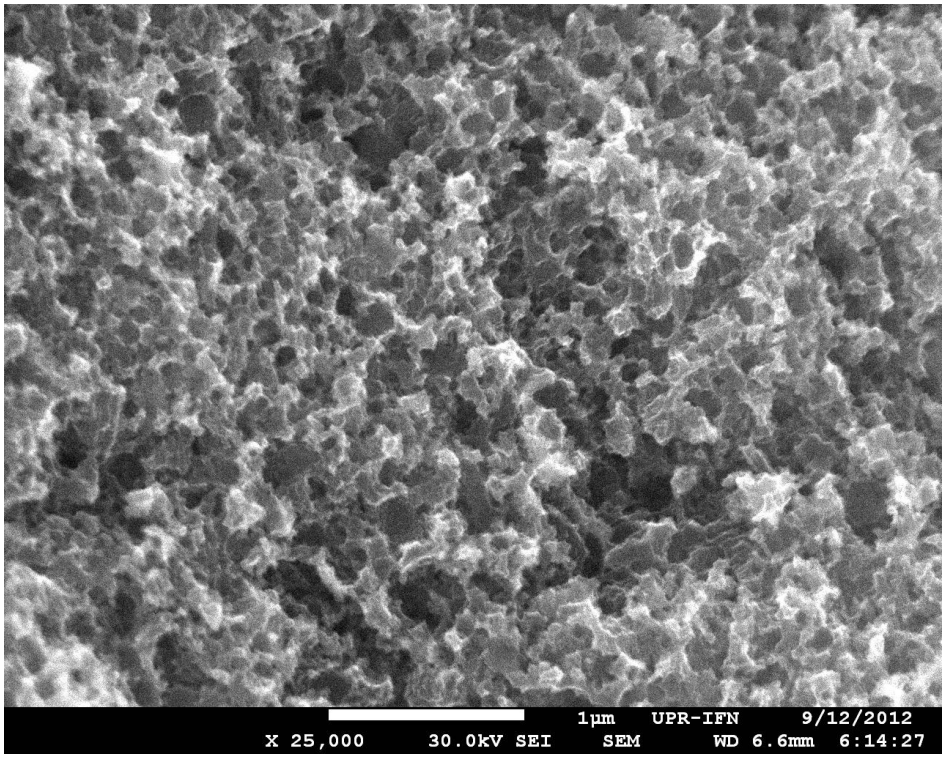

Figure 4.28 Al-25 at. % Zn alloy quenched into liquid nitrogen and electrochemically corroded in HNO_3. Magnification of black circle in figure 4.26.

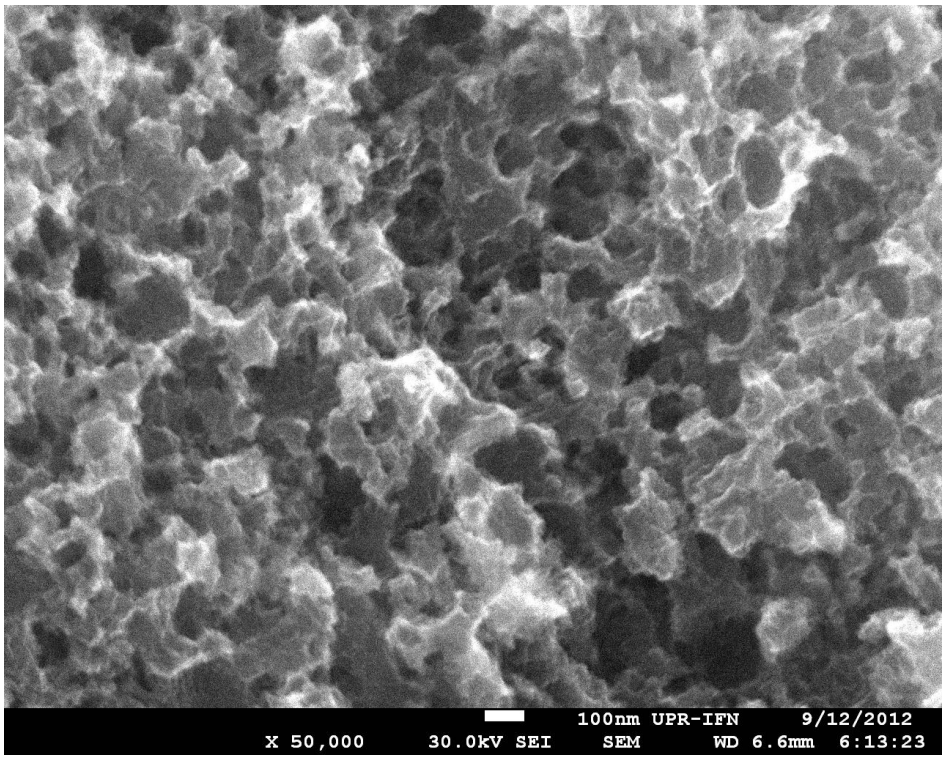

Figure 4.29 Al-25 at. % Zn alloy quenched into liquid nitrogen and electrochemically corroded in HNO_3. Magnification of black circle in figure 4.26. Interconnected ligament network with nano-sized pores can be observed.

5 CHARACTERIZATION

The fabrication of porous metals by chemical dealloying can be thought as using a chemical process to produce a specific physical result. This resulting porosity must be observed via microscopy because of its morphology and dimension restrictions. Section 4.2 discussed the fabrication of porous metals and the entire discussion has been based on SEM imaging, which was very useful for understanding of pore morphology, dendrite growth and cooling rate as well as zinc concentration effects. Nevertheless, additional evidence of the removal of aluminum and zinc by dealloying was needed. SEM imaging alone does not provide enough information to completely understand the selective removal. Another aspect that was of interest was the aluminum and zinc distribution inside the solid solution. This additional information was provided by two characterization techniques: X-ray diffraction and energy dispersive X-ray spectroscopy.

5.1 X-RAY DIFFRACTION

X-ray diffraction (XRD) was used to observe the effectiveness of corrosive media to selectively dissolve one of the species in the alloy. Since only two metals were used in the alloys, XRD provided sufficient evidence to identify their removal. A simple procedure was followed to complete the analyses. The characterization technique was applied to each sample, before and after corrosion. The characteristic diffraction peaks for each metal were then identified with the aid of a computer database containing powder diffraction files.

Figure 5.1 shows an XRD spectrum obtained from undealloyed 15 atomic percent of zinc alloy. Diffraction is a result of crystal reflection, thus independent of concentration. After all samples were analyzed, it was found that every non-corroded sample yielded similar spectrums. Miller indices of zinc and aluminum crystallographic planes are shown in red and blue respectively. This spectrum of undealloyed sample served as a benchmark to compare dealloyed sample diffraction patterns.

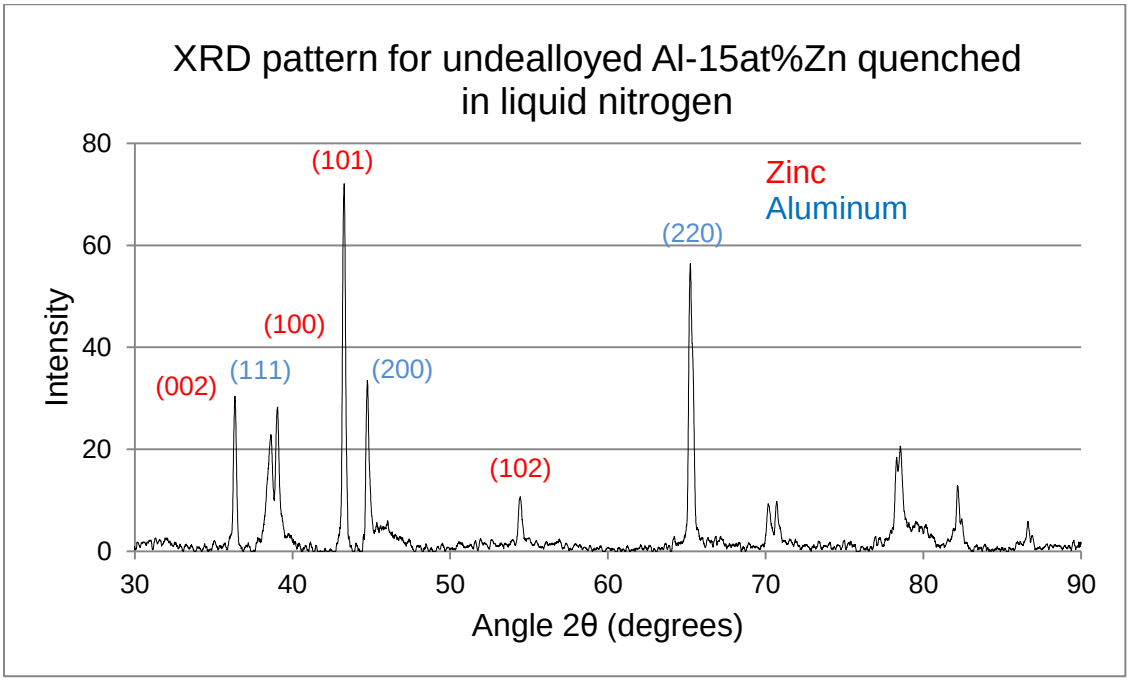

Figure 5.1 XRD diffraction pattern for undealloyed Al-15 at. % Zn. Both, aluminum and zinc characteristic peak are found. This diffraction chart represents a typical result for undealloyed samples.

The analysis of all diffraction patterns corroborated that sodium hydroxide had selectively removed aluminum and left zinc mostly untouched while nitric acid produced the opposite result. The diffraction patterns collected from samples corroded with NaOH were all very similar, with

differences only in peak intensities and widths. These differences are generated when fast cooling rates favored a zinc supersaturation in aluminum dendrites.

Figure 5.2 shows a typical X-ray diffraction pattern for an Al-Zn alloy corroded with NaOH. The characteristic peaks of zinc are evident while no aluminum peaks are found. This proves the effectiveness of NaOH to selectively remove aluminum. Even when concentration was changed to some extent, the resulting X-ray diffraction peaks were similar. Figure 5.3 is a diffractogram for Al-15 at. % Zn corroded in NaOH. As stated before, the main difference is the resulting peak intensities. Both patterns evince the complete removal of aluminum out of the alloy by NaOH.

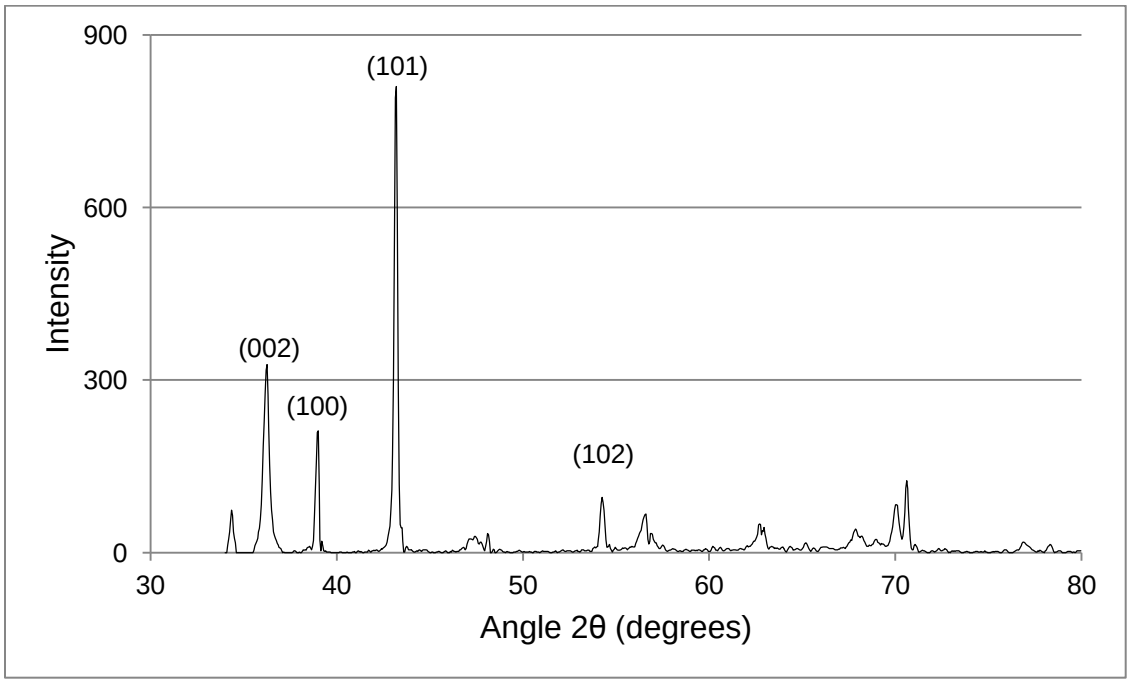

Figure 5.2 XRD pattern for Al-35 at. % Zn quenched in water and corroded in NaOH

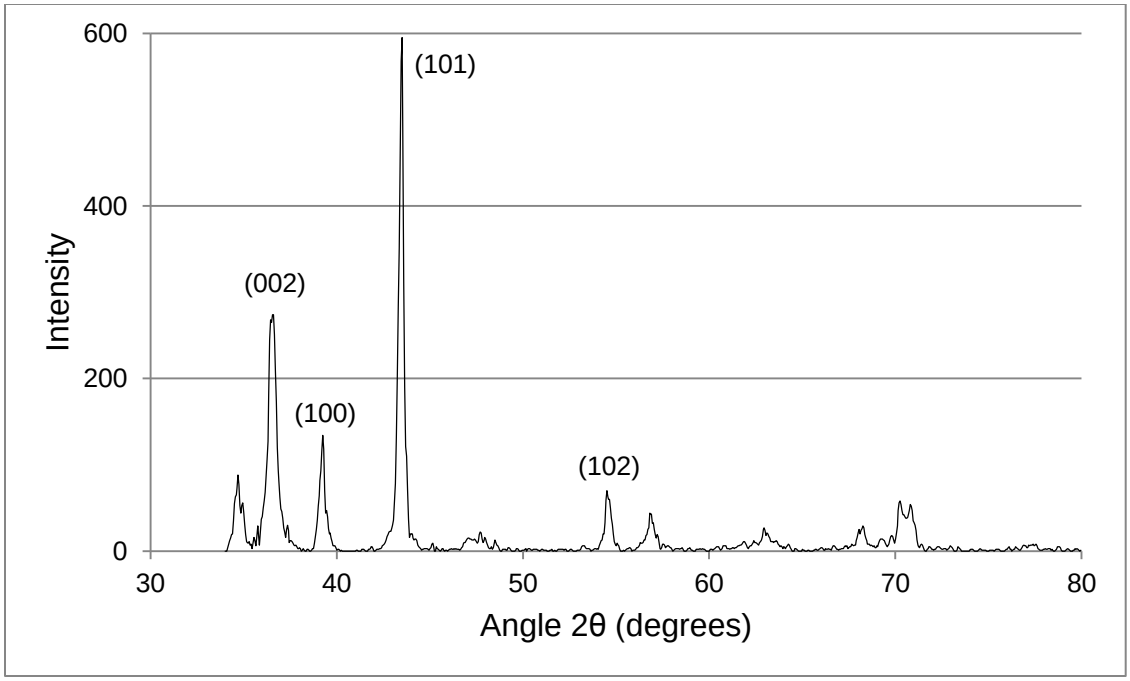

Figure 5.3 XRD pattern for Al-15 at. % Zn quenched in water and corroded in NaOH

When nitric acid was used as the corrosive medium to selectively dissolve the samples, an entirely different result was evident: the complete removal of zinc out of the alloy. The removal of zinc out of Al-Zn alloys with HNO_3 resulted strictly selective. As stated in section 4.2, NaOH affects, to some extent, both materials. When an Al-Zn alloy is treated with NaOH, their potential induces a preference for aluminum to be attacked first, even though zinc can also be dissolved. When using HNO_3 this does not occur. Aluminum does not dissolve readily in nitric acid but rather resists to the attack by passivation. This alloy behavior resulted in a very selective removal of zinc. Figure 5.4 shows a typical XRD pattern of an Al-Zn alloy corroded with nitric acid where complete removal of aluminum is evident. The characteristic peaks confirm the exclusive presence of aluminum in the sample.

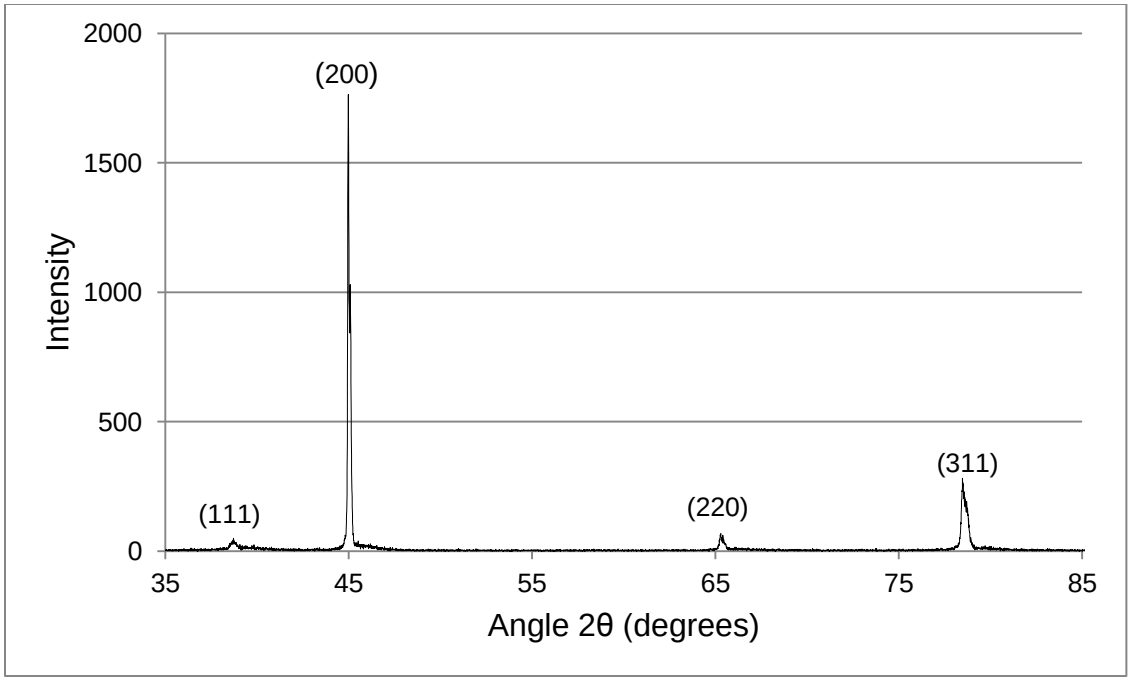

Figure 5.4 XRD pattern for Al-15 at. % Zn quenched in water and corroded in HNO_3

XRD analysis provided the necessary evidence to confirm the selective removal of species out of the alloys; nonetheless further data was needed to completely understand the dissolution of zinc in aluminum prior corrosion. Cooling techniques were applied to the samples to help induce the dissolution of zinc in aluminum-rich regions, thus promoting nanoporosity evolution inside dendrites. This dissolution of zinc atoms was observed using energy dispersive X-ray spectroscopy (EDS), as detailed in the following section.

5.2. ENERGY DISPERSIVE X-RAY SPECTROSCOPY

EDS can be used to determine the chemical composition of phases present in a material. When using EDS an incident beam removes electrons from their original high energy states, they then relocate in outer lower energy regions, emitting a specific signal. This signal is received and analyzed resulting in an accurate atomic identification. The typical data is arranged in a chart where intensity is a function of the radiation energy.

This technique was very helpful for the understanding of zinc solubility in aluminum. It was applied to a sample before and after corrosion. This study focused on the presence of zinc in the alloy. It was noticed that most of the zinc was forming a zinc-rich boundary surrounding the aluminum rich dendrites. It was also observed that some zinc was entering into the dendritic aluminum forming solid solution, and ultimately creating susceptible regions for the corrosion medium to attack. After corrosion, such spots become dimples which, depending on various factors, could grow into pores. It was noted that these dimples were forming mostly on the outer layers of the dendrites, indicating the importance of zinc supersaturation of the dendrites.

In order to understand the presence of zinc along the alloy, a zinc-rich inter dendritic region (figure 5.5), along with part of the neighbor dendrites, was selected to be studied using EDS. In that image two neighboring dendrites are adjacent to the zinc-rich boundary while many dimple precursors are evident. The yellow line in figure 5.5b indicates the EDS analysis line, while red and blue curves are the relative intensities for zinc and aluminum signals.

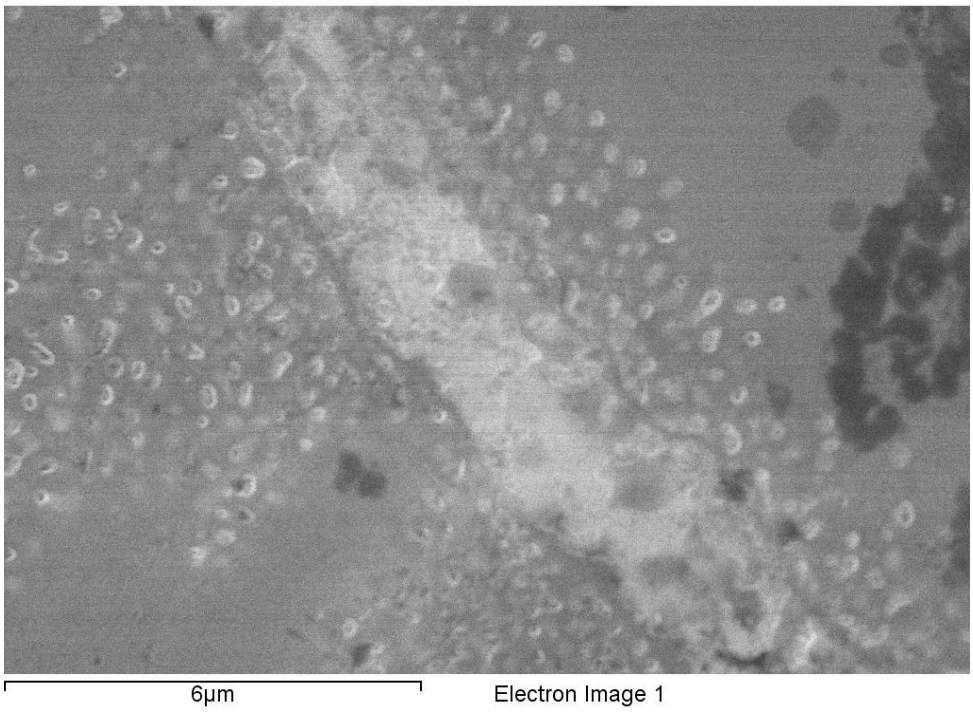

(a)

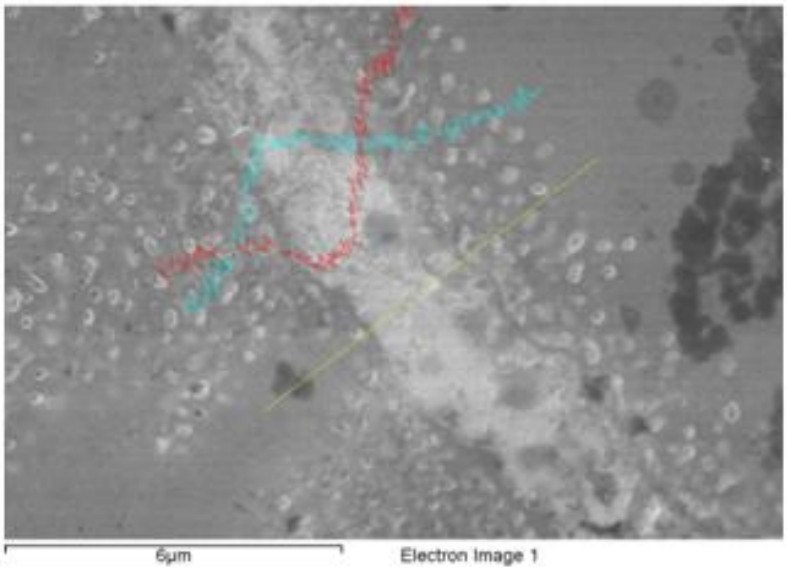

(b)

Figure 0.1 EDS analysis region for an Al-25 at. % Zn alloy without corrosion. The interface between aluminum and zinc rich areas was the region of interest.

The resulting spectrum revealed how zinc and aluminum were distributed along the analysis line. Figure 5.6 is the EDS spectrum for the sample in figure 5.5 where the red line represents the aluminum signal along the analysis line while the blue line represents zinc one. The first finding was that at the very center of the boundary, the zinc curve peaks while aluminum is at its lowest. Something worth noting is the fact that never a zero value was received for either element. Even in the zinc-richest parts, aluminum was detected. This might have two possible explanations: either aluminum is dissolved up to some extent in zinc, or the electron interaction region upon the EDS analysis is large and deep enough to produce signal from a deeper aluminum-rich region. We believe that the depth of analysis (5-7μm) is the responsible for this find. Also, aluminum has a very low solubility in zinc which makes it difficult for aluminum atoms to be dissolved in zinc-rich regions.

Another noteworthy aspect was that of high intensity of aluminum in dimple precursor regions. A closer look to figure 5.5b evinces the apparent high amount of dimple precursors on the right side of the analysis line and the also apparent lower amount of on the left side. However, if one observes the entire micrograph, one will notice that the dendrite on the left has a significantly higher amount of dimple precursor regions, while the right side dendrite only has a limited amount. This observation concurs with the fact that dimple precursor regions formation is a three-dimensional phenomenon. The left portion of the yellow line might not seem to be in a high density precursor region, while in reality, many of these precursors can be hidden.

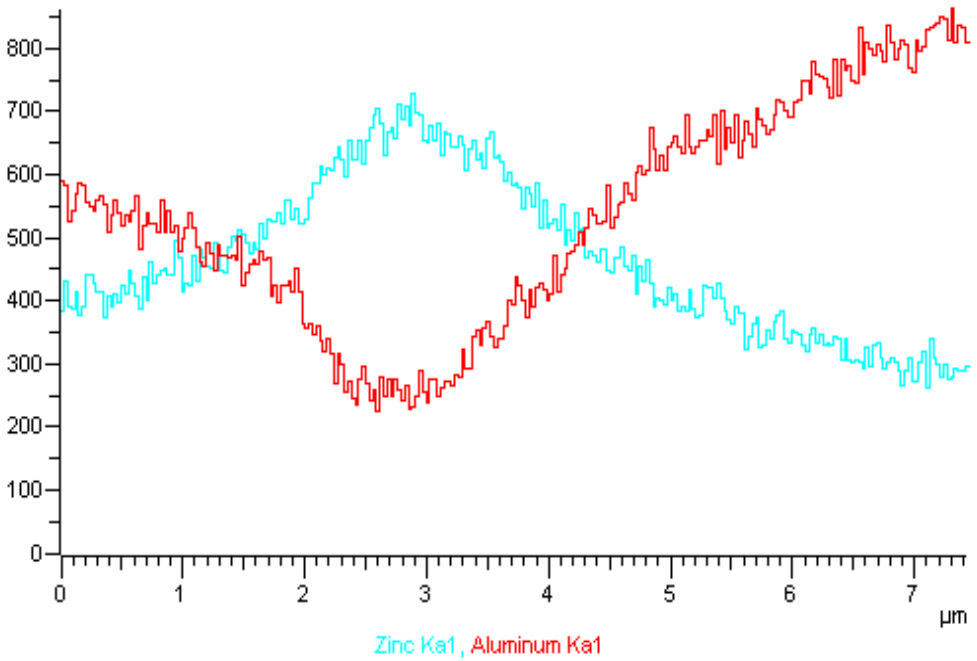

Figure 0.2 X-ray relative intensiy vs. distance for Al-25 at. % Zn alloy non-corroded. X axes represents the yellow line in figure 5.5b.

Figure 5.7 shows a small dendrite with large amounts of dimple precursor regions, which was selected for another EDS analysis to further corroborate these findings. The small, dendrite on the right side of the analyzed region is full of dimple precursor spots. Conversely, the left side of the analysis line bears very few precursor spots. The EDS analysis line was drawn crossing from the apparent low zinc region, across the zinc-rich boundary and finishing in the middle of the dendrite bearing numerous spots. Figure 5.8 is the resulting spectrum for this EDS analysis line. This time, the blue line represents aluminum while zinc is represented by red. Again a tendency for aluminum to decrease in the boundary region is observed and a tendency for zinc to do the same is observed inside the dendrites.

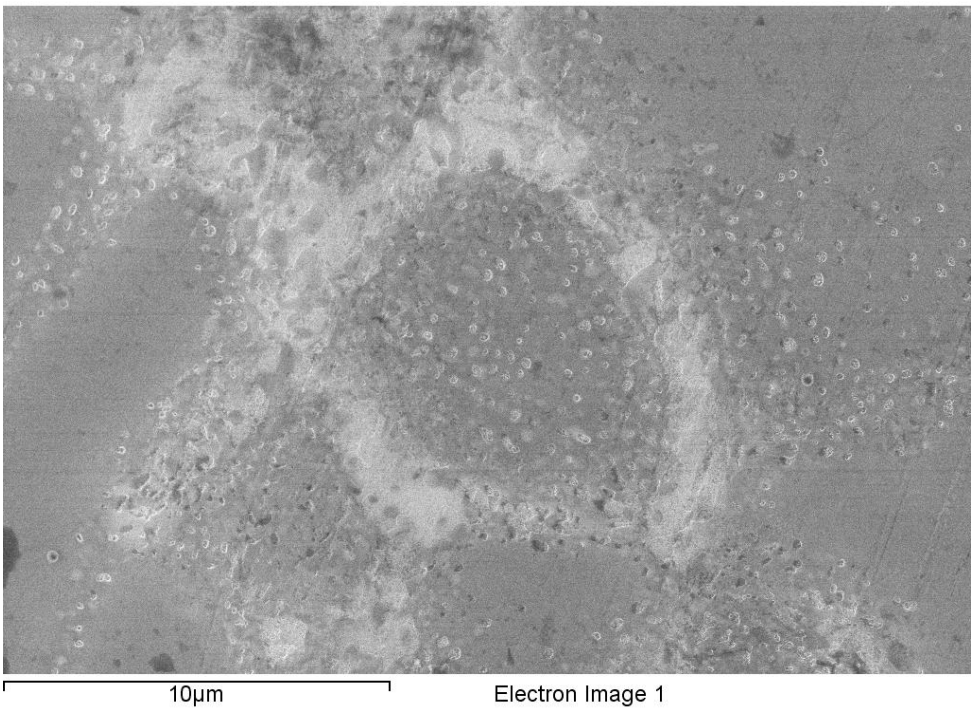

(a)

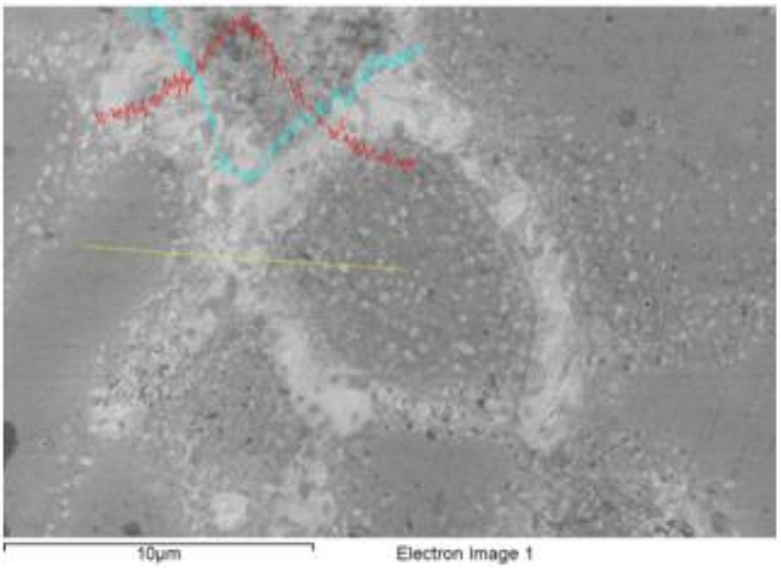

(b)

Figure 0.3 EDS analysis region for an Al-25 at. % Zn alloy without corrosion. The aluminum rich dendrite with dimple precursor regions was the region of interest.

In order to understand the distribution of zinc inside and around the outer regions of the dendrites, the following analysis is focused on both ends of the spectrum. Observing the left and right sides of the blue curve in figure 5.8 and comparing them with the left and right dendrites in

figure 5.7, a correlation between dimple precursor concentration and X-ray intensities can be inferred. The dendrite on the left seems to have very few dimple precursor spots while the aluminum X-ray intensity for this region is relatively high. Then, when observing the right dendrite and comparing it with the aluminum intensity curve, the same relationship is observed. The higher the amount of dimple precursor spots, the lower the relative aluminum intensity. It must be noted that the relative intensity for zinc on the right region is also lower than that on the left. This does not mean that such relationship between aluminum and dimple spots does not exists, but rather it tells that one should be looking at the curves trend more than their values.

It must be underscored how the blue line (aluminum) decreases from left to right. To some extent, the decreasing is a relatively sharp one as it comes closer to the boundary. Then, after the boundary, when the analysis line moves towards the center of the dendrite, the concentration profile line increases slowly. This fast decrease, horizontal movement and then slow increase can be safely related to the presence of dimple precursor spots. This form of the X-ray intensity lines might be indicating how zinc is actually distributed along the dendrite. This finding agrees perfectly with the solid solution and dendrite formation phenomena.

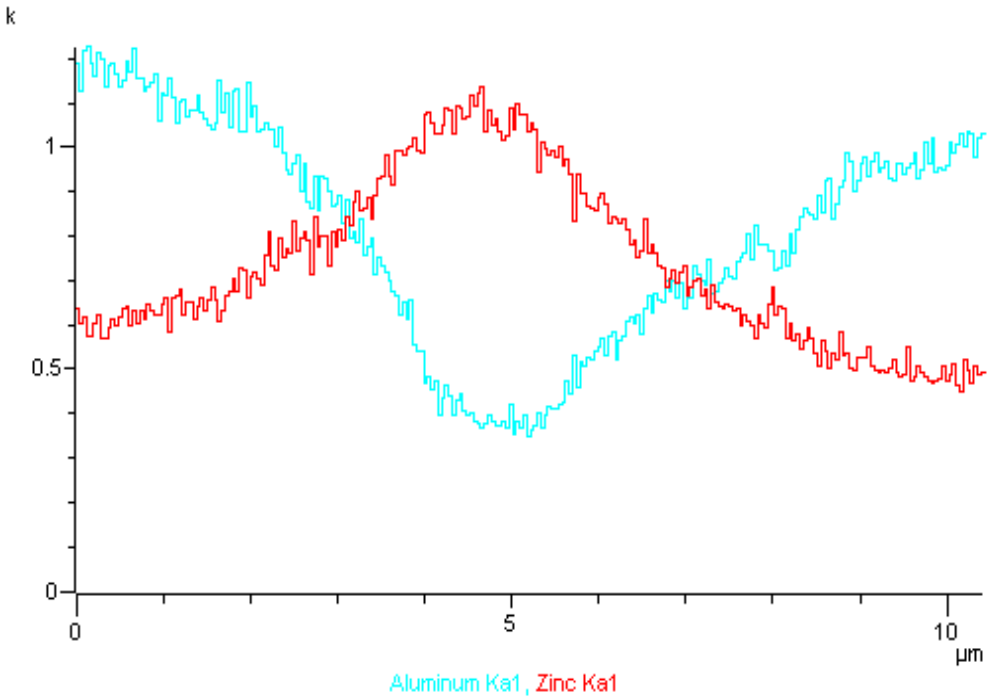

Figure 0.4 EDS spectrums for non-corroded Al-25 at. % Zn alloy.

EDS analyses confirm the presence of zinc inside dendrites while giving some insight of the overall general distribution of the species around dendrite boundaries. Nonetheless, one of the objectives of this analysis was to measure the presence or absence of the metals after corrosion. To this purpose, a similar alloy than those in figures 5.5 and 5.7 was electrochemically corroded with HNO_3. After corrosion, EDS analysis was applied to a similar dendrite boundary region, which was porous with roughly similar amount of dimples on both dendrites. Figure 5.9a is a micrograph of this region. Smaller pores can be observed on the upper and bottom parts of the image, as described in Section 4.2.2.2. Figure 5.9b shows the EDS analysis line, running from near the center of the left dendrite to near the center of the right one. This time the aluminum x-ray intensities are represented with blue lines.

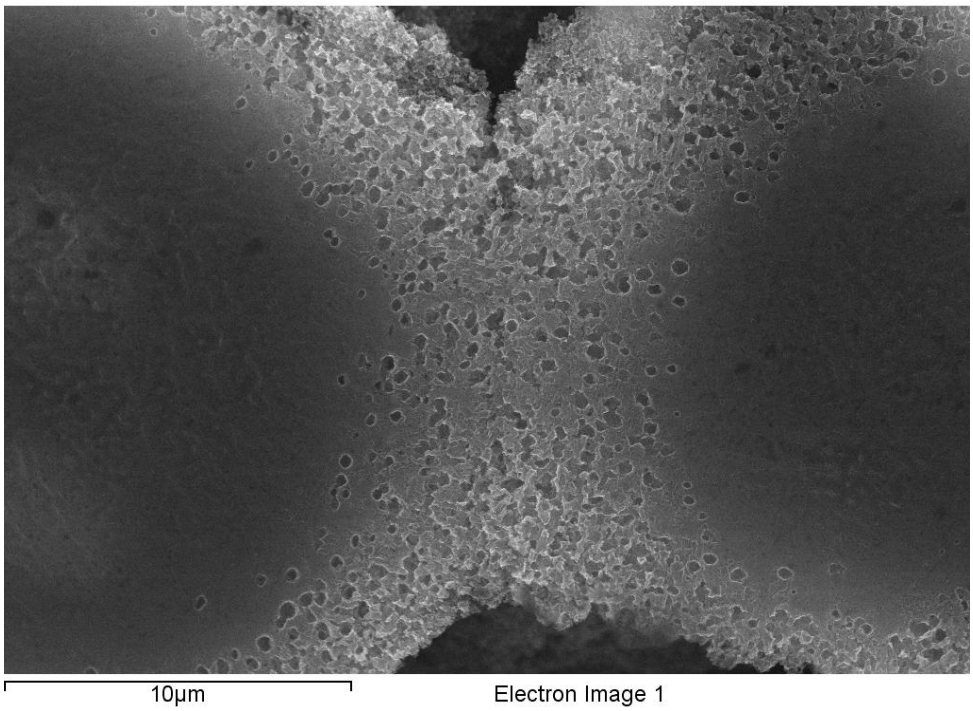

(a)

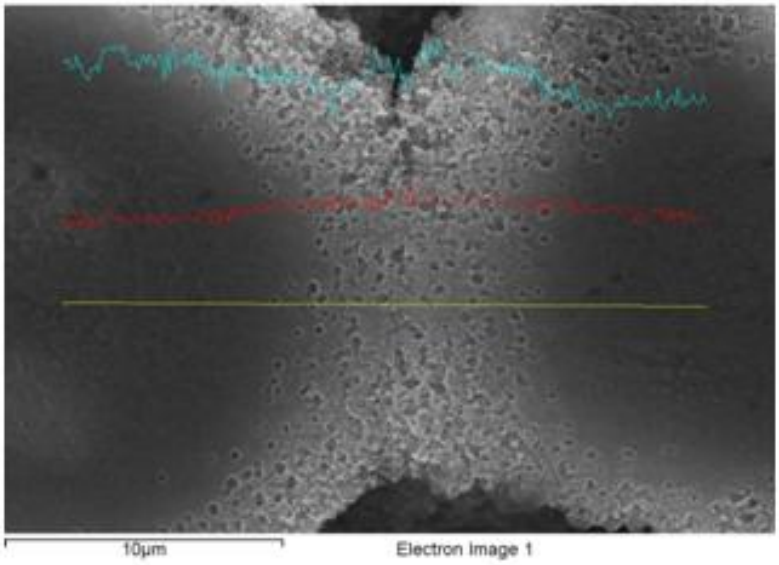

(b)

Figure 0.5 EDS analysis region for an Al-25 at. % Zn alloy selectively dissolved in HNO_3 solution.

Again, zinc intensity appears to increase in the boundary and decrease within the dendrites. Moreover, the aluminum spectrum does not behave with a particular trend, but rather varies constantly along the analysis line. Even though zinc trend is almost linear, it still follows the characteristic behavior of lower intensity ends. The scattering in the aluminum line might be the result of surface or subsurface porosity. The main finding from this analysis was the evidence of zinc presence after corrosion. It is important to notice that XRD analyses revealed the non extstence of zinc crystals after corrosion while here there is evidence of zinc. This indicates that the EDS-detected zinc must be actually dissolved in the passivated aluminum matrix.

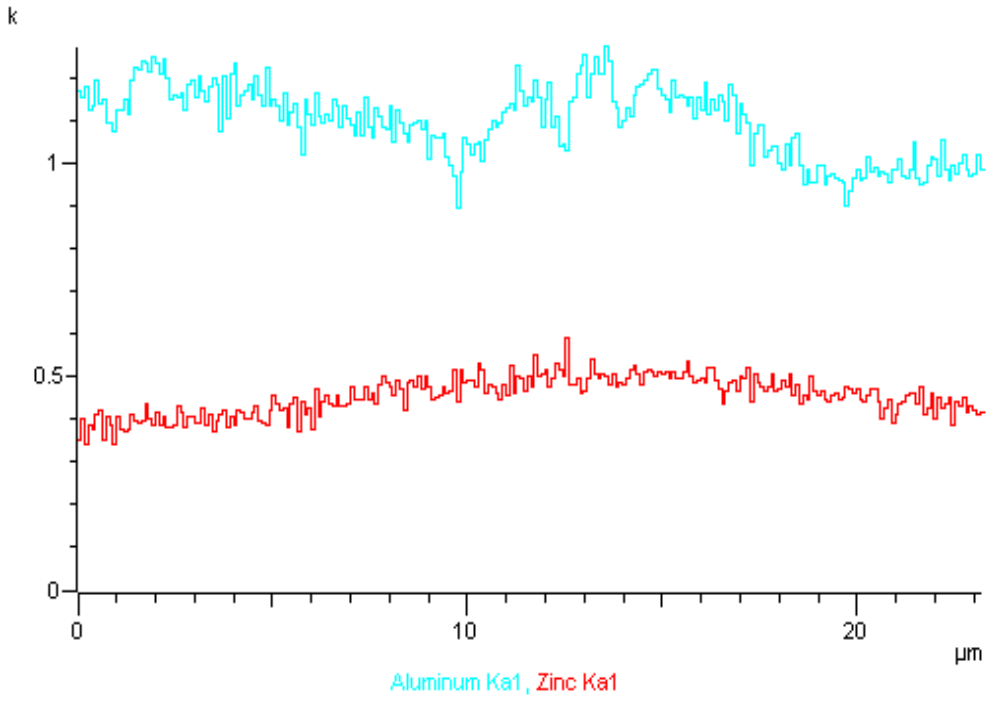

Figure 0.6 EDS spectrums for selectively dealloyed Al-25 at. % Zn alloy.

5.3 X-RAY MAPPING

Linear EDS analysis revealed the preferential presence of zinc in the interdendritic regions with some zinc present in the aluminum solid solution of the dendrites. As useful as this analysis is, the fact is the analysis line is composed of analysis points, which might not represent their surroundings; in other words this analysis does not provide a global distribution of the solute. In order to corroborate the linear EDS findings, another EDS analysis was implemented.

X-ray mapping is used to generate images of the elemental distribution on a sample surface. These images are produced by recording each analysis point's X-ray energy in a large surface grid. A color or brightness value is then assigned to each response to produce a digital image. Every element produces different X-ray photon energy, thus a different brightness or color.

Figure 5.11 is composed of three different images. The first one is a secondary electron image of an Al-25 at. % Zn alloy. This alloy was quenched with liquid nitrogen as a fast solidification method to retain the metastable presence of zinc supersaturating the aluminum-rich dendrites. In this image, dendrites and interdendritic regions are easily distinguishable. An EDS X-ray mapping analysis was then performed to observe the species distribution throughout the dendrites. The second image in figure 5.11 shows in red the distribution of aluminum throughout the sample. It is evident that aluminum is main phase in the dendrites, while it does not appear in large amount in the interdendritic regions.

The third image in figure 5.11 shows in green the places where zinc is located. It is evident that zinc is distributed all around the entire sample but not homogeneously. Zinc tends to concentrate in the interdendritic regions and the outer dendrite boundaries. This result is consistent with the preliminary linear EDS analysis.

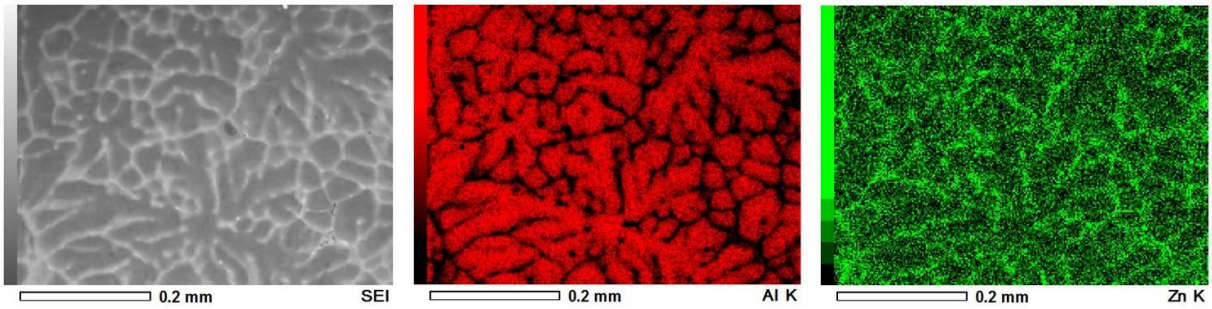

Figure 0.7 X-ray mapping of an Al-25 at. % Zn alloy quenched in liquid nitrogen. The sample was unetched.

Figure 5.12 shows the result of an X-ray mapping analysis applied to a dealloyed Al-25 at. % Zn alloy quenched in liquid nitrogen sample. The sample was also electrochemically attacked with nitric acid. Similar to figure 5.11, figure 5.12 shows the distribution of aluminum in red. Both images evince the aluminum-rich dendrites, although in figure 5.12, the red image seems sharper and more defined. The third image in figure 5.12 again shows in green the distribution of zinc. This time the removal of interdendritic zinc by selective dissolution is evident. It was also apparent some dissolved zinc remaining after corrosion. Selective dissolution has caused the removal of the interdendritic zinc while some dealloying might have dissolved some of the metastable zinc inside the outer dendrite regions. This dealloying could be causing the roughness of the outer dendrite layers and the formation of dimples. The passivation of aluminum by nitric acid may be preventing further dissolution of zinc. It is believed that the applied electrical potential could have helped the dissolution of surface and subsurface zinc.

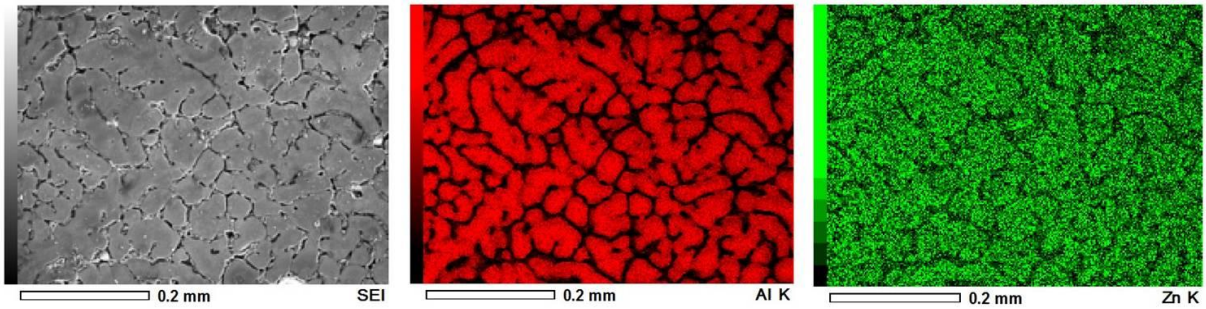

Figure 0.8 X-ray mapping of an Al-25 at. % Zn alloy quenched in liquid nitrogen and selectively dissolved with nitric acid and 1DC volt of electrical potential.

6 CONCLUSIONS AND SUGGESTIONS FOR FUTURE WORK

6.1 CONCLUSIONS

1. Porous aluminum and porous zinc were successfully fabricated using selective dissolution.
2. Pores with less than 100nm in diameter were observed in aluminum when selectively dissolved in HNO_3 with an applied electrical potential.
3. Selective removal of aluminum from Al-Zn alloys was successful using an aqueous solution of NaOH.
4. Selective removal of zinc from Al-Zn alloys was successful using an aqueous solution of HNO_3.
5. The application of an electric potential of 1 volt provided sufficient energy to the systems to alter the final porosity morphology. This was observed for both corrosive electrolytes, i.e. NaOH and HNO_3.
6. Fast cooling rates changed the microstructure of the samples and favored the dissolution of zinc atoms into the aluminum rich dendrites.
7. Results obtained from XRD analyses revealed the complete removal of zinc crystals when the Al-Zn alloys were treated with HNO_3. Moreover, a complete removal of aluminum phase was observed when the alloys were corroded in NaOH.
8. EDS results evinced the preferential distribution of zinc around the aluminum rich dendrites with some zinc atoms dissolved into the dendrites. The amount of zinc decreased towards the dendrite with a peak concentration outside the interface.

9. EDS analysis after HNO_3 corrosion revealed the presence of zinc atoms trapped inside the aluminum rich dendrites. This concurs with the XRD results of complete removal of zinc crystals, but evinces some remaining zinc.
10. Dimple formation was a result of corroded zinc-rich spots inside the outer layer of the dendrites. When two dendrites were close enough to share a zinc boundary, dimples favored the formation of secondary porosity resulting interconnection of growing dimples.
11. Nanoporosity evolution could be happening in aluminum-rich dendrites were aluminum atoms diffuse to permit the selective removal of zinc. This might occurred for Al-Zn alloys quenched in liquid nitrogen and corroded in HNO_3.
12. No evidence of nanoporosity evolution was observed on the samples corroded with NaOH.
13. The smallest pores created under this work were macropores ranging from 50 to 100nm in diameter. These were created on Al-25 at. % Zn quenched in liquid nitrogen and electrochemically corroded in HNO_3.
14. The optimal concentrations in the Al-Zn system to fabricate porous metals were 25 and 35 at. % zinc in aluminum, approximately 45 and 57 wt. % zinc respectively. This concurs with the literature were scientists recommend a roughly 50/50 wt. % alloy to create porous metals.

6.2 SUGGESTIONS FOR FUTURE WORK

In this work, porous aluminum and porous zinc were fabricated using chemical dealloying or selective dissolution. To our knowledge, no other work has ever been done on this topic using these alloys and corrosive solutions. To a large extent, this work has been a novel one following the scientific method whenever possible. Nevertheless, the premature general scientific knowledge on fabrication of porous aluminum and zinc by selective dissolution, made of this pioneer research a hard process, leaving many desirable variables without being investigated. The following is a list the author suggests for future works.

1. Use different electrolyte solutions to observe their effect on porosity morphology and nanoporosity evolution. It would also be desirable to study the effect of higher and lower concentrations of NaOH and HNO_3.
2. Since the alloy concentrations selected represented a proof-of-concept approach, further analysis on other chemical compositions must be done.
3. Since the application of electric potential increased the formation of smaller pores it is suggested that higher voltages be applied to observe their effect.
4. As the measurement of real potentials of the metals should help understanding the dealloying process this should be done with reference electrodes.
5. Fast cooling rates provided the needed microstructures to create nanopores. These rates were not directly measured in this work, but approximated using a SDAS vs. cooling rate chart. It is suggested to accurately measure the cooling rates and to identify which phenomenon is responsible for the apparent slow cooling of liquid nitrogen. The possible explanations were described but were not proven.

6. Surface area is one of the most important terms in skeletal catalysis. In order to completely characterize our porous metals, a method of surface area measurement should be used.
7. Another characterization method that would help understanding the morphology of porosity is transmission electron microscopy (TEM)
8. Since one of the main applications for these materials is catalysis, the author suggests identifying possible reactions where these metals act as catalysts and to investigate the possible functionalization of the porous metals.

7 REFERENCES

[1] J. Erlebacher and R. Seshadri, “Hard Materials with Tunable Porosity,” *MRS Bulletin*, vol. 34, no. August, 2009.

[2] J. Erlebacher and J. Schwarz, “Dealloying of Binary Alloys: Evolution of Nanoporosity,” in *Encyclopedia of Nanoscience and Nanotechnology*, 2004.

[3] A. J. Smith, “Skeletal Catalysts,” in *Surface and nanomolecular catalysis*, 2006.

[4] H. Qiu, C. Xu, X. Huang, Y. Ding, Y. Qu, and P. Gao, “Immobilization of Laccase on Nanoporous Gold: Comparative Studies on the Immobilization Strategies and the Particle Size Effects,” *The Journal of Physical Chemistry*, vol. 113, pp. 2521-2525, 2009.

[5] S. O. Kucheyev, J. R. Hayes, J. Biener, T. Huser, C. E. Talley, and A. V. Hamza, “Surface-enhanced Raman scattering on nanoporous Au,” *Applied Physics Letters*, vol. 89, no. 5, 2006.

[6] Murray Raney, “Method of preparing catalytic material,” U.S. Patent 15635871925.

[7] Murray Raney, “Method of producing finely-divided nickel,” U.S. Patent 16281901927.

[8] H. W. Pickering, “Electrolytic Dissolution of Binary Alloys Containing a Noble Metal,” *Journal of The Electrochemical Society*, no. July 1967, pp. 698-706, 1967.

[9] J. Weissmüller, R. C. Newman, H.-jun Jin, A. M. Hodge, and J. W. Kysar, “Nanoporous Metals by Alloy Corrosion□: Formation and Mechanical Properties,” *MRS Bulletin*, vol. 34, no. August, pp. 577-586, 2009.

[10] A. J. Forty, “Corrosion micromorphology of noble metal alloys and depletion gilding,” *Nature*, vol. 282, no. 5739, pp. 597-598, Dec. 1979.

[11] J. Erlebacher, M. J. Aziz, a Karma, N. Dimitrov, and K. Sieradzki, “Evolution of nanoporosity in dealloying.,” *Nature*, vol. 410, no. 6827, pp. 450-3, Mar. 2001.

[12] M. Hakamada and M. Mabuchi, “Microstructural evolution in nanoporous gold by thermal and acid treatments,” *Materials Letters*, vol. 62, no. 3, pp. 483-486, Feb. 2008.

[13] Q. Zhang, X. Wang, Z. Qi, Y. Wang, and Z. Zhang, “A benign route to fabricate nanoporous gold through electrochemical dealloying of Al–Au alloys in a neutral solution,” *Electrochimica Acta*, vol. 54, no. 26, pp. 6190-6198, Nov. 2009.

[14] Z. Zhang, Y. Wang, Z. Qi, C. Somsen, X. Wang, and C. Zhao, “Fabrication and characterization of nanoporous gold composites through chemical dealloying of two phase Al–Au alloys,” *Journal of Materials Chemistry*, vol. 19, no. 33, p. 6042, 2009.

[15] R. Zeis, T. Lei, K. Sieradzki, J. Snyder, and J. Erlebacher, “Catalytic reduction of oxygen and hydrogen peroxide by nanoporous gold,” *Journal of Catalysis*, vol. 253, no. 1, pp. 132-138, Jan. 2008.

[16] H. Siyu et al., “The preparation of nanoporous gold electrodes by electrochemical alloying/dealloying process at room temperature and its properties,” *Materials Letters*, vol. 64, no. 21, pp. 2296-2298, Nov. 2010.

[17] E. Seker et al., “The effects of post-fabrication annealing on the mechanical properties of freestanding nanoporous gold structures,” *Acta Materialia*, vol. 55, no. 14, pp. 4593-4602, Aug. 2007.

[18] H. Zhou, L. Jin, and W. Xu, “New approach to fabricate nanoporous gold film,” *Chinese Chemical Letters*, vol. 18, no. 3, pp. 365-368, Mar. 2007.

[19] S. G. Corcoran and W. T. Reynolds, “Nanoporous platinum,” 2003.

[20] M. Hakamada and M. Mabuchi, “Preparation of nanoporous Ni and Ni–Cu by dealloying of rolled Ni–Mn and Ni–Cu–Mn alloys,” *Journal of Alloys and Compounds*, vol. 485, no. 1–2, pp. 583-587, Oct. 2009.

[21] Z. Qi, C. Zhao, X. Wang, J. Lin, W. Shao, and Z. Zhang, “Formation and Characterization of Monolithic Nanoporous Copper by Chemical Dealloying of Al-Cu Alloys,” vol. 90, no. condition I, pp. 6694-6698, 2009.

[22] M. Hakamada and M. Mabuchi, “Fabrication of nanoporous palladium by dealloying and its thermal coarsening,” *Journal of Alloys and Compounds*, vol. 479, no. 1–2, pp. 326-329, Jun. 2009.

[23] T. Aburada, J. M. Fitz-Gerald, and J. R. Scully, “Synthesis of nanoporous copper by dealloying of Al-Cu-Mg amorphous alloys in acidic solution: The effect of nickel,” *Corrosion Science*, vol. 53, no. 5, pp. 1627-1632, May 2011.

[24] W. B. Liu, S. C. Zhang, N. Li, J. W. Zheng, and Y. L. Xing, “A facile one-pot route to fabricate nanoporous copper with controlled hierarchical pore size distributions through chemical dealloying of Al–Cu alloy in an alkaline solution,” *Microporous and Mesoporous Materials*, vol. 138, no. 1–3, pp. 1-7, Feb. 2011.

[25] X. Peng, K. Koczkur, S. Nigro, and A. Chen, “Fabrication and electrochemical properties of novel nanoporous platinum network electrodes.,” *Chemical communications (Cambridge, England)*, vol. 1, no. 24, pp. 2872-3, Dec. 2004.

[26] W. B. Liu, S. C. Zhang, N. Li, J. W. Zheng, and Y. L. Xing, “Influence of phase constituent and proportion in initial Al–Cu alloys on formation of monolithic nanoporous copper through chemical dealloying in an alkaline solution,” *Corrosion Science*, vol. 53, no. 2, pp. 809-814, Feb. 2011.

[27] C. Zhao, Z. Qi, X. Wang, and Z. Zhang, “Fabrication and characterization of monolithic nanoporous copper through chemical dealloying of Mg–Cu alloys,” *Corrosion Science*, vol. 51, no. 9, pp. 2120-2125, Sep. 2009.

[28] J. Zhou, “Porous Metallic Materials,” in *Advanced Structural Materials*, CRC Press, 2006, pp. 103-124.

[29] L. An-Hui, *Nanocasting□: a versatile strategy for creating nanostructured porous materials*. Royal Society of Chemistry, 2010.

[30] H. Masuda and K. Fukuda, “Ordered metal nanohole arrays made by a two-step replication of honeycomb structures of anodic alumina.,” *Science (New York, N.Y.)*, vol. 268, no. 5216, pp. 1466-8, Jun. 1995.

[31] Y. Ding and M. Chen, “Nanoporous Metals for Catalytic and,” vol. 34, no. August, 2009.

[32] H. Baker, Ed., “Alloy Phase Diagrams,” in *ASM Handbook, Volume 3*, .

[33] T. Wada, K. Yubuta, A. Inoue, and H. Kato, “Dealloying by metallic melt,” *Materials Letters*, vol. 65, no. 7, pp. 1076-1078, Apr. 2011.

[34] F. Group, “Forms of Metallic Corrosion,” pp. 27-76, 2010.